ADVANCED QUANTUM TECHNOLOGIES
www.advquantumtech.com

Chirped Pulses Meet Quantum Dots: Innovations, Challenges, and Future Perspectives

*Florian Kappe, Yusuf Karli, Grant Wilbur, Ria G. Krämer, Sayan Ghosh, René Schwarz, Moritz Kaiser, Thomas K. Bracht, Doris E. Reiter, Stefan Nolte, Kimberley C. Hall, Gregor Weihs, and Vikas Remesh**

Shaped laser pulses have been remarkably effective in investigating various aspects of light–matter interactions spanning a broad range of research. Chirped laser pulses exhibiting a time-varying frequency, or quadratic spectral phase, form a crucial category in the group of shaped laser pulses. This type of pulses have made a ubiquitous presence from spectroscopic applications to developments in high-power laser technology, and from nanophotonics to quantum optical communication, ever since their introduction. In the case of quantum technologies recently, substantial efforts are being invested toward achieving a truly scalable architecture. Concurrently, it is important to develop methods to produce robust photon sources. In this context, semiconductor quantum dots hold great potential, due to their exceptional photophysical properties and on-demand operating nature. Concerning the scalability aspect of semiconductor quantum dots, it is advantageous to develop a simple, yet robust method to generate photon states from it. Chirped pulse excitation has been widely demonstrated as a robust and efficient state preparation scheme in quantum dots, thereby boosting its applicability as a stable photon source in a real-world scenario. Despite the rapid growth and advancements in laser technologies, the generation and control of chirped laser pulses can be demanding. Here, an overview of a selected few approaches is presented to tailor and characterize chirped pulses for the efficient excitation of a quantum dot source. By taking the chirped-pulse-induced adiabatic rapid passage process in quantum dot as an example, numerical design examples are presented along with experimental advantages and challenges in each method and conclude with an outlook on future perspectives.

1. Introduction

Rapid advancements in laser technology in the past decades have resulted in the development of various methods to control the properties of laser pulses. From a simple intensity control to the generation of complex waveforms, many of these methods have contributed remarkably to our understanding of light–matter interactions.[1–3] For comprehensive reviews on pulse shaping techniques, see refs. [4–7].

A major player in the family of shaped laser pulses is the one with the instantaneously varying frequency, called chirped laser pulse.[8] Such type of laser pulses have found immense applications in various scientific fields, for instance, to coherently control atomic and molecular energy transition pathways, [9–18] manipulating nanoscale nonlinear optical resonances,[19–21] laser pulse amplification[22,23] enabling the generation of laser pulses of extremely high peak power, cavity optomechanics,[24] fiber optic communication,[25] signal processing,[26,27] breakdown process in dielectric materials,[28] to name a few.

In quantum technologies, too, chirped laser pulses have been employed

F. Kappe, Y. Karli, S. Ghosh, R. Schwarz, M. Kaiser, G. Weihs, V. Remesh
Institut für Experimentalphysik
Universität Innsbruck
Technikerstraße 25d, 6020 Innsbruck, Austria
E-mail: vikas.remesh@uibk.ac.at

G. Wilbur, K. C. Hall
Department of Physics and Atmospheric Science
Dalhousie University
Halifax, Nova Scotia B3H 4R2, Canada

R. G. Krämer, S. Nolte
Institute of Applied Physics, Abbe Center of Photonics
Friedrich Schiller University Jena
07745 Jena, Germany

T. K. Bracht
Institut für Festkörpertheorie
Universität Münster
Wilhelm-Klemm-Straße 10, 48149 Münster, Germany

The ORCID identification number(s) for the author(s) of this article can be found under https://doi.org/10.1002/qute.202300352

DOI: 10.1002/qute.202300352

successfully. The possibility to coherently transfer the population to specific quantum states is of paramount importance in developing future applications.[29] Semiconductor quantum dots are arguably one of the most important sources for generating bright, photostable, and high-quality quantum light states on-demand.[30,31] The past decade has witnessed remarkable achievements in terms of photon rate, purity, and entanglement fidelity.[32,33] Specifically in thecase of state preparation in semiconductor quantum dots, chirped pulses have proven particularly effective, for instance see refs. [34–40]. The ability to tune the chirp allows for selective excitation of specific electronic states, paving the way for new stable and efficient sources of high-purity single-photons and entangled photon states. To this end, generating, controlling, and characterizing chirped pulses for experiments on quantum emitters with high precision can be technically demanding and overwhelming, given that diverse methods have been developed over the past few years. As a result, there is a clear need to appreciate the characteristics of available methods from a practical viewpoint.

This overview article is arranged as follows: starting with a brief introduction to chirped pulses, we present an illustrative example on the relevance of chirped pulses in quantum dot excitation. We then turn our attention to experimental techniques to prepare and characterize chirped pulses, with the current state of the art in each technique and emphasizing practical design examples and insights. Finally, we present an outlook with future prospects of chirped pulse control in quantum dot research and technological applications.

2. Chirped Pulses: Basics

A linearly chirped laser pulse can be described in the frequency domain as

$$E(\omega) = E_0 \exp\left[-\frac{(\omega-\omega_c)^2}{\Delta\omega^2}\right] \exp\left[i\frac{\phi_2}{2}(\omega-\omega_c)^2\right] \quad (1)$$

where E_0 is the amplitude of the Gaussian frequency envelope centred at ω_c with a frequency bandwidth of $\Delta\omega$ and ϕ_2 describes the group delay dispersion (GDD). Applying a Fourier transform to Equation (1) leads to the time domain representation of this laser pulse modulated with a linear chirp, given by

$$E(t) \propto \tilde{E}_0 \exp\left[-a_c t^2\right] \exp\left[-i(\omega_0 + bt)t\right] \quad (2)$$

where a_c is related to τ_p, the duration of resultant chirped pulse (given as the full with at half maximum, FWHM, of the pulse intensity) as $a_c = \frac{2\ln 2}{\tau_p^2}$, and b denotes the chirp rate in time given by $b = 2\phi_2/[\tau_0^4/(2\ln(2))^2 + (2\phi_2)^2]$ where τ_0 represents the transform-limited pulse duration. It is obvious that the instantaneous frequency of the laser pulse varies as $\omega(t) \to \omega_0 + bt$. Therefore, introducing ϕ_2 has two effects: it stretches the temporal duration of the laser pulse from τ_0 to τ_p according to the relations $\tau_p^2 = \tau_0^2 + (\frac{4\ln 2\phi_2}{\tau_0})^2$ and $\tilde{E}_0 \propto E_0/\sqrt{\tau_p\tau_0}$, and dictates the frequency ordering in the pulse. For positive ϕ_2, the frequency increases over time, meaning the red part (longer wavelength) of the spectrum arrives before the blue part (shorter wavelength) and vice versa for negative ϕ_2. In **Figure 1**, we illustrate how the concept of chirped pulses reciprocates in spectro-temporal domains.

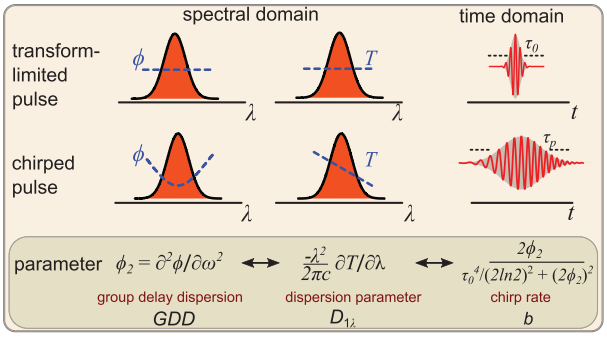

Figure 1. Representation of transform-limited and chirped pulses in spectral and time domains. *T*- wavelength-dependent time delay, τ_0- duration of the transform-limited pulse, τ_p- duration of the chirped pulse, *b*- chirp parameter.

By definition, the GDD is the second derivative of the spectral phase ϕ with respect to the angular frequency ω, or the first derivative of group delay (T) with respect to angular frequency. That is

$$\phi_2 = \mathrm{GDD} = \frac{\mathbf{d}^2\boldsymbol{\phi}}{\mathbf{d}\boldsymbol{\omega}^2} = \frac{\partial T}{\partial\omega} = D_2(\omega) \quad (3)$$

The dispersion parameter $D_{1\lambda}$ (in units of ps nm^{-1}) is related to GDD (in units of ps^2) through

$$D_{1\lambda} = \frac{\partial T}{\partial\lambda} = -\frac{2\pi c}{\lambda^2}\cdot\frac{\mathbf{d}^2\boldsymbol{\phi}}{\mathbf{d}\boldsymbol{\omega}^2} = -\frac{2\pi c}{\lambda^2}\cdot\mathrm{GDD} \quad (4)$$

It is now clear that a positive GDD implies a shorter time delay for the red part of the laser spectrum and vice versa for negative GDD.

3. Chirped Pulses for Quantum Dots

In semiconductor quantum dots, the optical excitation to the exciton state is followed by the emission of single photons, and the biexciton state results in the emission of entangled photon pairs. For excellent reviews on various excitation methods of quantum dots, see refs. [30, 41, 42]. The most popular method of optical driving is the resonant excitation to either the exciton or the biexciton state. Here, a laser pulse with its central frequency tuned to the transition energy of the quantum dot, drives the system resonantly with its signature Rabi frequency. This is usually evidenced by the so-called Rabi rotations as one sweeps the excitation pulse area[41,43] (see black curve in **Figure 2**a, bottom

T. K. Bracht, D. E. Reiter
Condensed Matter Theory, Department of Physics
TU Dortmund
Otto-Hahn-Straße 4, 44227 Dortmund, Germany
S. Nolte
Fraunhofer Institute for Applied Optics and Precision Engineering IOF
Center of Excellence in Photonics
07745 Jena, Germany

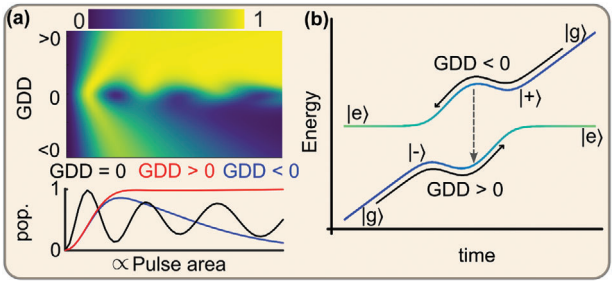

Figure 2. Robustness of ARP: a) Simulated excited state occupation as a function of pulse area and GDD, at low temperatures. The line cuts correspond to zero (black), positive (red), and negative (blue) GDD, respectively. b) Dressed state energies of a two-level system during the ARP process. Colours indicate the overlap with the ground state (|g⟩, blue) and the excited state (|e⟩, green). The dashed arrow represents phonon emission during ARP with GDD < 0.

panel). However, an important attribute of quantum dot photon sources is their spectral variability, induced by the growth process itself.[44,45] This is usually on the order of 5 nm. From a practical viewpoint, this distribution in emission wavelengths offers a possibility to produce *frequency-multiplexed* single-photons and entangled photon pairs. Yet, the sensitivity of Rabi rotation to spectral (i.e., Rabi resonance) and spatial variation (i.e., the dipole coupling) makes it ineffective in a practical scenario.

Chirped laser pulses mitigate this issue by relaxing the resonance requirement, relying on the so-called Adiabatic Rapid Passage (ARP). In Figure 2a, we illustrate the effect of chirped pulse excitation of a quantum dot. In this two-dimensional map of the simulated excited state occupation (at low temperatures) as a function of pulse area and GDD, one can identify three main regimes, represented by the linecuts in the bottom panel. For zero chirp (black curve), one observes the resonant Rabi rotations in the excited state population. For large positive GDD (red curve), the excited state population reaches a plateau, and does not show any dependence on pulse area, while for large negative GDD, the population reaches a maximum, and then drops to low values for high pulse areas. The latter effect is due to the interaction with *phonons*, that is, lattice vibrations, pertinent to quantum dots, which causes a deterioration of the ARP process.

The ARP process is well understood in the dressed state picture, which reveals the adiabatic nature via an avoided energy level crossing,[46,47] see Figure 2b. As the instantaneous laser frequency is swept across the quantum dot resonance – provided it is sufficiently slow compared to the Rabi frequency – the evolution of the system becomes adiabatic. If this process is faster than the characteristic relaxation time of the excited state(s), one obtains a smooth population inversion.[47] Depending on the sign of the chirp, the system will evolve via either the low or high-energy dressed state, depicted by the arrows along the branches in Figure 2b. For GDD > 0, the graph has to be read from left-to-right, starting and ending in the lower branch. Conversely, for GDD < 0, the graph has to be read from right-to-left, as the different ordering of the frequencies in the pulse can also be understood as a time-reversal. As long as no dressed-state transitions occur during the excitation pulse, the system will evolve adiabatically from the ground to the excited state.

For low temperatures, where only phonon *emission* processes play a role, the efficiency of the ARP process depends on the sign of the chirp[48] (see Figure 2b). For GDD < 0, the maximum state preparation efficiency varies depending on the chosen GDD and pulse area, as phonon emission processes lead to transitions from the upper to the lower branch, depicted by the dashed arrow in (b). In contrast, for GDD > 0, the excited state preparation efficiency achieves nearly unity efficiency for all powers > 2.5 π, as the system traverses the lower branch, avoiding phonon emission. Therefore, for efficient excitation of a single quantum dot, positively chirped excitation is preferred. At higher temperatures, phonon *absorption* processes increasingly start to play a role in quantum dots, also degrading the preparation fidelity. Note that at higher laser powers, there exists a regime of phonon decoupling, where the sign of the chirp does not influence the population inversion as observed in refs. [49, 50]. The ARP process has been exploited for quantum dot excitation by several groups including ours,[34–36,38–40,51–53] targeting both the excitonic and the biexcitonic states. In **Table 1**, we have compiled a list of experimental and theoretical demonstrations of ARP in various platforms.

Historically evolved from the atomic and molecular spectroscopy research, over the past decade, the ARP excitation has enlarged its scope to quantum dot technologies and its practical implementation. For the optical driving of a quantum dot *ensemble*, the ARP method, different from all the other coherent excitation techniques,[30,41,42] offers the additional advantage that it is immune to spatio-spectral fluctuations. The robustness of ARP against spectral detuning has been demonstrated by targeting exciton states in single and multiple quantum dots at telecom[54,55] and infrared wavelengths.[40] This is important, for instance to generate frequency-multiplexed, high-purity photons from a quantum dot sample without compromising the excitation efficiency, and without the need for having a site-selective excitation pulse control.

For experimental illustration of the robustness of ARP excitation in the case of a quantum dot ensemble, in **Figure 3a** we describe the ARP excitation process on two different quantum dot platforms: GaAs/AlGaAs quantum dot emitting around 800 nm, and InGaAs/GaAs quantum dots with emission around 1300 nm. For the former, we employ two-photon excitation targeting the biexciton state, while for the latter, we rely on the p-shell excitation. Both methods have the advantage that the emitted photons can be spectrally filtered. In the case of two-photon excitation, the advantages are that the emitted photons are entangled states, and that it offers the highest single-photon purities achievable (see refs. [30, 56] for an overview). For p-shell excitation, the advantage is that it permits the use of broadband laser pulses (i.e., short in time) which enables ultrafast control of quantum states.[38] Specifically in the case of ARP-induced robustness, the chirped *two-photon excitation* can afford a quantum dot spectral variability (with excited state preparation efficiency > 95%) of ≈ 1.5 meV,[40] while in the chirped *p-shell excitation*, the affordable range can be as large as 10 meV,[54,55] which is the typical spectral variability in a quantum dot ensemble. Therefore, the choice of excitation can be decided by the quantum dot system employed and the overall goal.

Ever so often, complex experimental techniques are often accompanied or even led by theoretical descriptions and predictions of at least equal complexity. Therefore, extensive efforts have been

Table 1. Overview of the works demonstrating adiabatic rapid passage in various emitter systems.

Experiment	References	Method	System	Maximum Chirp
General theory	For eg. [43, 47]	–	–	–
QD theory	For eg. [48, 49, 63–66]	–	–	–
Atomic and molecular systems	For eg. [67–70]	Grating stretcher	Na and I_2 vapour, Rb atom	≈ 15 ps^2 [67–69], ≈ 0.2 ps^2 [70]
QD exciton	[34, 35, 52, 71, 72]	Grating stretcher and glass rods	InGaAs QD around 940 nm	-40 ps^2 [34], 11 ps^2 [35], 0.3 ps^2 [71], 30 ps^2 [52], 30 ps^2 [72]
QD biexciton	[39, 40, 53]	Grating stretcher [39, 40], CFBG [53], CVBG [this work]	InGaAs QD around 940 nm [39], GaAs QD around 800 nm [40, 53]	≈ ±0.3 ps^2 [39], 45 ps^2 [40, 53], 90 ps^2 [this work]
QD p-shell	[38, 50, 54, 55]	SLM	InGaAs QD around 1270 nm	0.13 ps^2 [38], 0.3 ps^2 [54, 55]
Notch-filtered AP	[73]	SLM	InGaAs QD around 1270 nm	0.15 ps^2 [73]
Coupled QD	[74, 75]	Theoretical work	–	–
Piecewise AP	[76]	Theoretical work	–	–

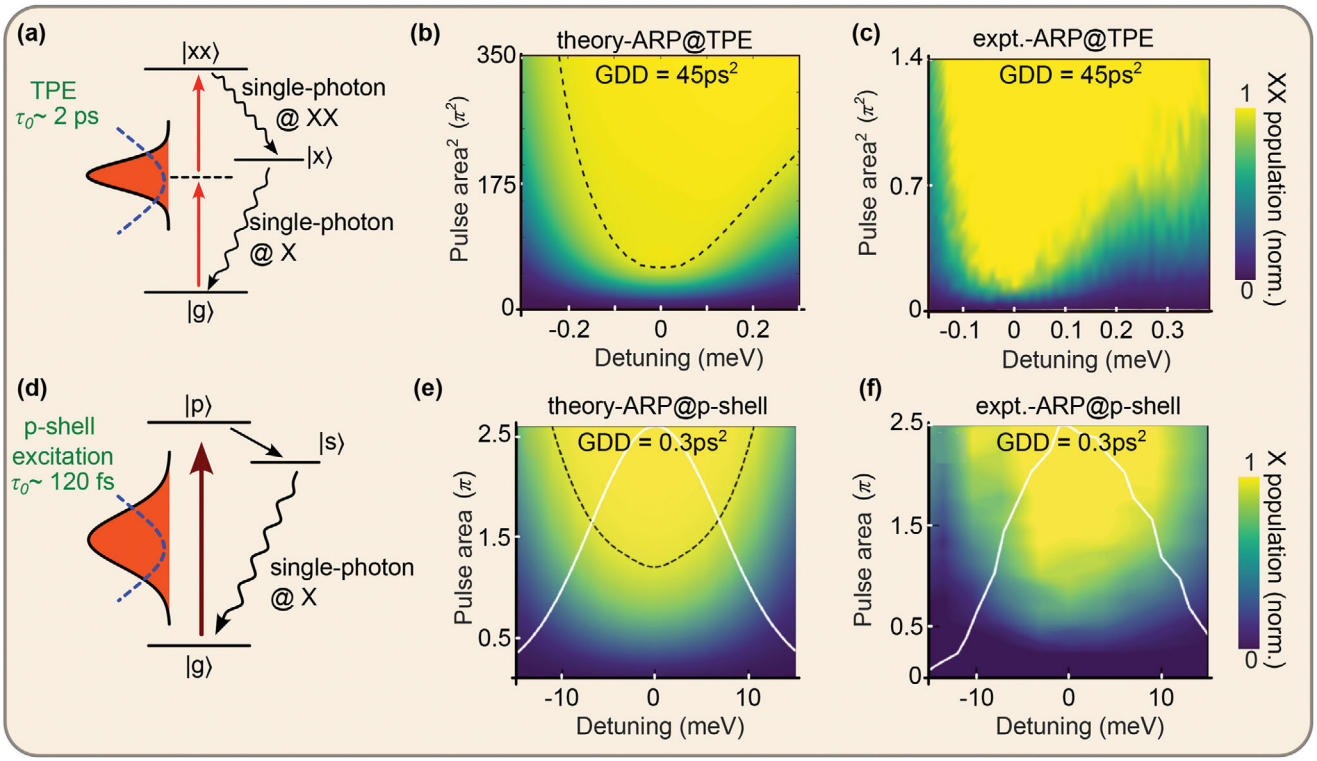

Figure 3. Chirped pulse excitation of quantum dots: a) A quantum dot three-level system composed of ground state (|g⟩), exciton state (|x⟩), and biexciton state (|xx⟩) subjected to chirped *two-photon excitation* (TPE). b) Simulated two-dimensional map of the variation in biexciton population as a function of the laser energy detuning and pulse area in a single quantum dot, for GDD = 45 ps^2, that is, at the ARP condition. c) Experimental results of (b). d) A three-level system composed of ground state (|g⟩), s-shell exciton state (|s⟩), and the p-shell exciton state (|p⟩) undergoing chirped *p-shell excitation*. e) The simulated two-dimensional map of the variation in s-shell exciton population as a function of detuning and pulse area for GDD = 0.3 ps^2, that is, at the ARP condition. The white curve indicates the used laser spectrum. The black, dashed contour lines represent the corresponding 95% exciton occupation under *TPE* and *p-shell excitation*. f) Experimental results of (e). Parts (e) and (f) are adapted with permission.[54] The Optical Society 2021.

invested in providing a comprehensive theoretical understanding of the ARP and related effects in quantum dots, a description of which is beyond the scope of this article. For a description on the model Hamiltonian, see refs. [40, 42]. To simulate the quantum dot dynamics, we employ a process tensor matrix product operator (PT-MPO) method, as elaborated in refs. [57–60]. This method, along with path integral approach,[61] offers the capability to include the phonon environment in a numerically complete fashion. For other theoretical methods, see also refs. [54, 62].

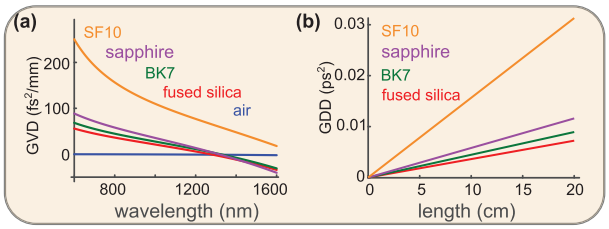

Figure 4. Materials for dispersion control: a) Dispersion properties of commonly employed materials calculated from corresponding Sellmeier coefficients. b) Achievable GDD at 800 nm using these materials as a function of the propagation distance.

4. Experimental Techniques of Pulse Chirping

Experimentally, chirped pulses have been produced by various methods, each having its own advantages and disadvantages. In this section, we illustrate the features of a few of them highlighting the pros and cons, efficiency, and numerical examples to help design and implement each. Note that this list is by no means exhaustive, and a selection has been made, considering the trivialities of quantum dot excitation techniques. To complement, in Section 5, we have also provided an overview of characterization methods addressing chirped pulses.

The simplest method of all is to utilize materials with $\frac{d^2n(\lambda)}{d\lambda^2} \neq 0$, with $n(\lambda)$ being the wavelength-dependent refractive index, commonly described with Sellmeier equations.[77] Positive GDD is accumulated upon propagation in all transparent materials in the visible wavelength range, while it becomes negative (or anomalous) in the near-infrared wavelengths. This dispersion causes different wavelengths in a broadband laser pulse to travel at different velocities, causing a temporal stretching of the laser pulse, that is, chirp. The phase acquired by propagating a distance of L_d in a medium of refractive index n can be calculated from

$$\frac{d^2\phi}{d\omega^2} = L_d \frac{\lambda^3}{2\pi c^2}\frac{d^2n}{d\lambda^2} = L_d \cdot \mathrm{GVD} \tag{5}$$

with

$$\mathrm{GVD} = \frac{\lambda^3}{2\pi c^2}\frac{d^2n}{d\lambda^2} \tag{6}$$

being the *Group Velocity Dispersion* [78]. By propagating a laser pulse through a sufficiently long medium of high GVD, one can add an arbitrary amount of dispersion to it. In **Figure 4a**, we present commonly employed dispersive materials along with their GVD in the wavelength range 600–1600 nm and in (b) we present the achievable GDD for propagation lengths up to 20 cm in these materials.

The significance of GDD on a laser pulse depends on the frequency bandwidth, or conversely, the pulse duration of the laser source, and its central frequency. Consider a 10 mm BK7 glass, which carries a GDD of around 500 fs^2. A 10 fs pulse centred around 800 nm propagating through this block will disperse to 100 fs, while a 100 fs pulse *only* stretches to 102 fs. On the other hand, in fiber-based dispersion method, for instance, the dispersion parameter $D_{1\lambda}$ of silica at 800 nm is about 100 ps nm^{-1} km^{-1}. Propagating a 100 fs pulse through a 20 m fiber results in a GDD of 0.7 ps^2, which stretches it to 20 ps. All of these mean that the requirement of dispersion and its controllability (i.e., the sign, magnitude and so on) in the ARP experiment and the quantum dot spectral range determine the material employed. If one uses a 2 ps-long laser pulse to perform the ARP experiment (see refs. [40, 53, 64]), the required chirp is nearly 45 ps^2. For such high dispersion requirements, most of the options in Figure 4 are not suitable, due to the resulting propagation lengths and corresponding losses specifically in the case of fibers at near-infrared wavelengths. On the other hand, for few cycle pulses, these are valuable tools, in some cases also to characterize the pulses.[79,80] For dispersion up to 15000 fs^2, monolithic elements such as chirped mirrors[81,82] are also useful components.

4.1. Grating Stretchers

Historically, the most popular method to impart high values of GDD has been grating stretcher (for positive chirp) and compressor (for negative chirp). They operate based on wavelength-dependent optical path length differences induced by the angular dispersion of gratings. The simplest scenario is a parallel grating pair separated by a distance, called Treacy configuration.[83]

The GDD produced by a grating pair can be calculated via the formula

$$\phi_2 = \frac{-\lambda_0^3 L}{\pi c^2 d^2}\left[1 - \left(\frac{\lambda_0}{d} - \sin\theta_i\right)^2\right]^{-3/2} \tag{7}$$

where L is the separation between the gratings, θ_i is the angle of incidence, d the grating period (1/groove density), λ_0 the central wavelength and c the speed of light. It is obvious that the GDD (including the sign) can be varied by tuning the separation between the gratings. Note that, in the Treacy configuration, regardless of the grating separation, grating period, or angle of incidence, the dispersion remains negative. Based on this principle, grating pairs were originally used for the purpose of pulse compression in high-power laser research.[84] However, by introducing a negative magnification telescope between the grating pair, which allows for negative values of L in Equation (7) (and switching from parallel to anti-parallel grating orientation), one can reverse the sign of dispersion. This is called the Martinez stretcher (hereafter referred to as "grating stretcher"), demonstrated with detailed mathematical analysis in refs. [84–88].

The grating stretcher is essentially a 4f shaper[6] but double-passed. In the first pass, the wavelength components are dispersed, and the time delay between the wavelength components is introduced by deviating from the zero dispersion configuration. In the second pass, the dispersion is further added while the spatial spread is undone. The expression for the grating stretcher dispersion (Equation (7)) establishes that to impart a large GDD, one needs a large grating separation L, which results in a large spatial dispersion of the spectral components. To mitigate this, one can implement the folded version using a single grating, lens, a roof prism, and a folding mirror at the back focal plane of the lens.[89,90] In this configuration, after the first two passes, the beam is retroreflected back to the stretcher and propagates the same path again. To tune the GDD, the stage (combining grating and roof prism) is translated, with the input, diffracted, and

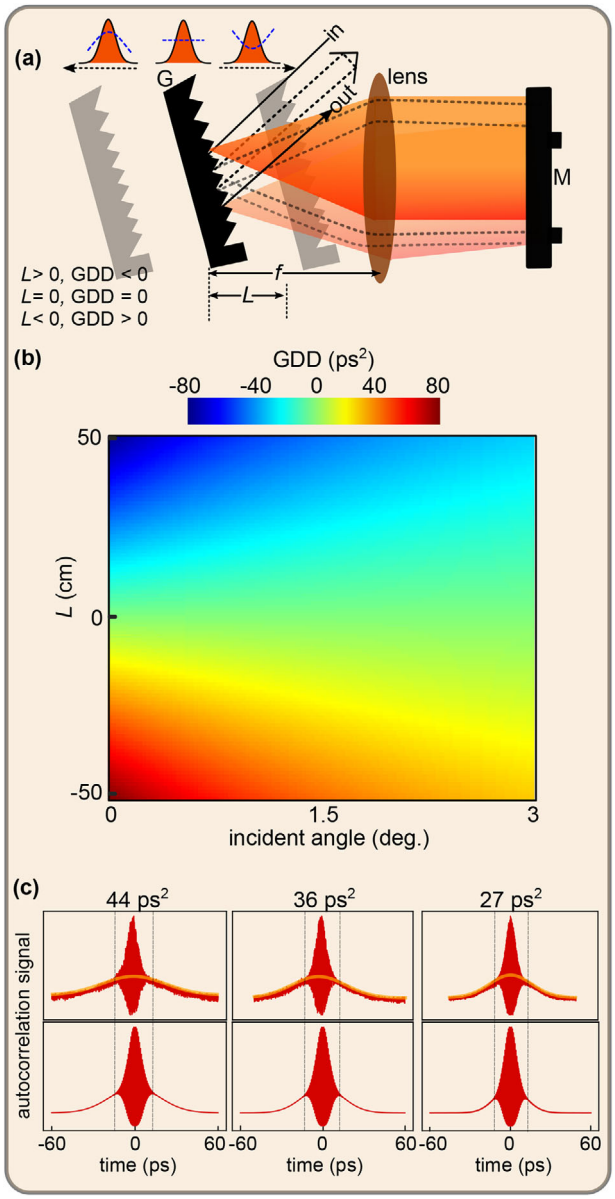

Figure 5. a) Grating stretcher designed in a folded, quadruplex configuration. Incoming and outgoing beam paths are indicated, along with the direction of translation of the grating to impart non-zero GDD. G- grating, M- flat mirror, *L*- effective grating separation in Equation (7). b) Sensitivity of the grating stretcher as evidenced by the simulated two-dimensional map of GDD as a function of the grating separation *L* and angle of incidence. c) Interferometric autocorrelation traces recorded for various *L* in the grating stretcher, with corresponding measured (upper row) and simulated (lower row) GDD values indicated.

output beams kept parallel. Finally, the outgoing beam acquires the desired GDD. The overall footprint is reduced to half, yet with the same dispersion properties as in the regular design. In **Figure** 5a, we sketch the design of a folded, *quadruple-pass* grating stretcher employed in refs. [40, 91]. One can also add additional phase and amplitude masks to provide further shaping capabilities in a grating stretcher.[92,93]

Practical Considerations: Gratings suffer from third and fourth-order dispersions in addition to the desired GDD. In principle these can be compensated by careful designs,[94] yet, it increases the experimental complexity. Due to its design, grating stretchers are known to be sensitive to various misalignments, which have been studied extensively in refs. [95–105]. One of the critical issues in the regular, unfolded design is the non-parallelism of gratings. This results in residual angular chirp (which in turn produces pulse front tilts). Additionally, the telescope lens alignment in the grating stretcher is critical, as any aberrations here will contribute to the imperfect reversal in the dispersion sign. In a folded design, on the other hand, critical issues include the off-axis passage through the lens. This gives rise to chromatic aberration and astigmatism, affecting the output fiber coupling. In both cases, one might need additional telescope correction: be it for an optimized coupling to a single-mode fiber, or to reduce spurious spatiotemporal artifacts in actual experiments. Note that, in either case, the deviation δx of the folding mirror from the Fourier plane has to be kept $\delta x \ll f^2/L$.[91]

In addition to the distance tuning, Equation (7) stipulates that by tuning the angle of incidence, dispersion tuning is achieved. It is sometimes necessary to use the grating at grazing incidence to obtain the required high value of GDD,[40] at the expense of diffraction efficiency and the net power throughput. In Figure 5b, we display the simulated two-dimensional map of the GDD as a function of the incident angle at the grating θ_i and *L*. It is evident that for a fixed position of grating with respect to the focussing lens, tuning θ_i by <1° results in a drastic variation in GDD. In fact, this feature adds to the complexity of the alignment procedure in a grating stretcher.

Consider an experiment as described in Figures 3c and 3f, that is, where the laser pulses with varying GDD are produced to excite a quantum dot. To achieve this, the grating and the roof prism (see the design schematics in refs. [89, 90]) have to be moved to corresponding distances from the lens. Due to the alignment sensitivity, one needs to adjust the grating angles, recalibrate the GDD, and iteratively run an output power optimization with the beam correction telescope. Additionally, as established in Figure 2a, due to the sensitivity of the excitation method, one needs to ensure that the laser spectrum matches the quantum dot resonance. More importantly, the experiments with negative GDD will increase the footprint even further, as the grating assembly has to be moved away from the focal plane of the lens. An overview of the grating stretcher-based chirping, highlighting its major features, is presented in **Table 2**. To qualitatively characterize the chirp at various positions of the grating, we utilized interferometric autocorrelation (for details see Section 5), and the recorded traces are displayed in Figure 5c, upper row, along with the simulated ones in Figure 5c, lower row, showing good agreement with each other.

Efficiency: The total free-space power throughput of a grating stretcher strongly depends on the grating diffraction efficiency η_{grating},

$$\eta_{\text{grating stretcher}} = \eta_{\text{grating}}^4 \tag{8}$$

because the laser beam hits the grating(s) at least four times. Additionally, for an efficient output single-mode fiber coupling,

Table 2. Summary of the advantages and disadvantages of grating-based stretcher designs.

Grating stretchers for chirping	
Advantages	Disadvantages
• Broad wavelength operation • Variable GDD possible by simple translation • Customizable for arbitrary wavelengths	• Bulky and prone to mechanical instabilities • Throughput strongly depends on the grating efficiency • Beam distortions and aberrations present • Spectral clipping for large beam sizes • Challenging alignment for aberration-free design • Negative chirp option increases the footprint

one needs to incorporate beam-correction methods.[106] By employing custom-designed, high-efficiency gratings, and iterative beam correction routines the power throughput can be improved but is still limited by the physical constraints described earlier. We note that a stretcher can also be constructed using prisms, yet grating pairs provide, for a given separation, much greater dispersion with respect to prism pairs and are thus suitable for introducing large-frequency chirps.

Example Design: For a GDD of 45 ps^2, a grating stretcher can be constructed in folded geometry.[40] Consider a laser pulse centred around $\lambda_0 = 795$ nm, a grating with a groove density 1200 grooves/mm and a lens with $f = 75$ cm. If the grating efficiency is 70%, the ideal throughput of the system will be 24%. Due to the expected spread in spatial profile, grating dimensions should be at least 50 mm. For an effective distance $L = 55$ cm (and double-passed), at Littrow configuration ($\approx 28°$), the GDD is only 4 ps^2. As illustrated in Figure 3a–c, this is not sufficient to achieve ARP under two-photon excitation. Therefore, to achieve a GDD of 45 ps^2, the angle of incidence has to be chosen $\theta_i = 2°$,[40] for the same grating. With a higher groove density grating and a corresponding Littrow angle of $\approx 46°$ one can achieve 20 ps^2, which is still insufficient for the experiments described in refs. [40, 53].

4.2. Spatial Light Modulators

The advent of liquid crystal technologies has given rise to electronically addressable digital modulators, of which the most widely used is the spatial light modulator (SLM). They are liquid crystal-based cells exhibiting voltage-dependent birefringence. The orientation of the liquid crystal molecules in each cell can be controlled electronically. As a result, for a given polarization of the incoming light, applying voltage can introduce phase retardation or a combination of phase retardation and polarization rotation. There are several types of SLMs commercially available: one-dimensional SLMs based on nematic liquid crystals,[6,107] or two-dimensional SLMs based on liquid crystal on Silicon (LCOS) technology.[108] The major difference between the two in terms of design is that the former has two transmissive substrates enclosing a nematic liquid crystal layer, whereas LCOS SLM makes a double-pass through one transmissive substrate in addition to the dielectric-coated pixels. For a detailed description of the operating principles, see refs. [6, 107, 108]. In LCOS SLMs, one of the substrates is constituted by a Silicon backplane which consists of all the electronic circuitry. In the scope of this article, we only consider transmissive, one-dimensional SLM (hereafter termed "1D-SLM") and reflective phase-only LCOS SLMs (hereafter called "2D-SLM").

To enable a simultaneous phase and amplitude shaping of laser pulses, the SLM is mounted at the Fourier plane of a 4*f* shaper. In the case of 1D-SLMs[109–111] one requires a dual-mask configuration where the phase imparted is the difference of retardance between the two masks and the amplitude function is the sum[6,107] of the two. A 2D-SLM, however, utilizes the principle of diffractive pulse shaping[112–114] to perform simultaneous phase and amplitude shaping.[115,116] Here, the SLM generates a phase grating and diffracts light in different orders, whose intensity and phase can be tuned by changing the modulation depth and the frequency of the grating pattern projected. A 1D-SLM-based 4*f* shaper can be constructed either in a single-pass or a folded double-pass configuration. The former ensures higher power throughput at the cost of a challenging alignment procedure (see the discussion on the grating stretcher), while the latter offers twice the phase modulation with half the number of optical elements.

In **Figure 6**, we sketch the basic operation of an SLM-equipped 4*f* shaper encompassing a 1D SLM (Figure 6a) arranged in a non-Littrow configuration while in Figure 6b we present a 2D SLM-based system constructed in Littrow configuration. In a 2D SLM-based shaper, the horizontal axis corresponds to the spectral spread and the phase masks are projected along the vertical direction. In a 1D-SLM-based shaper, the pixel drive levels corresponding to quadratic phases are modulated along the spectral axis. In either case, to generate chirped pulses,[38,109,117–119] initially, a precise phase-voltage calibration is performed, from which a lookup table is generated, where every phase is related to a precise drive voltage. Following this, a wavelength calibration is prepared to map individual pixels to appropriate wavelength components, dictated by the resolution of the shaper. Based on these two, a quadratic spectral phase profile (either 1D or 2D) can be applied across the required pixels, corresponding to the appropriate wavelength range that needs to be addressed. For radiation in the visible range, the maximum phase modulation varies from 2π to 4π, depending on the exact spectral range and SLM.

In Figure 6c, we show a representative sketch of a chirp phase mask (blue curve) projected on an SLM where a 2 ps laser pulse (with intensity spectrum shown as green shaded area) is spread on. To confirm the generation of the chirped pulse, we directed the outgoing beam from the 4*f* shaper to an interferometric autocorrelation setup (details in Section 5, and see Figure 6d). The simulated trace for a 10 ps^2 pulse (shown as inset in Figure 6d) shows a good agreement with the measurement.

Practical Considerations: Compared to grating stretchers, the advantage of SLM-based pulse chirping is the programmability enabling the generation of arbitrary spectral and temporal profiles. Despite its elegance and simple functionality, some aspects need a careful look in the SLM-based pulse-chirping setups.

As the spectral phase of a chirped pulse is proportional to ω^2 (see Equation (1)), and given that the SLM is a pixellated device, continuous phase functions are approximated by discrete steps.

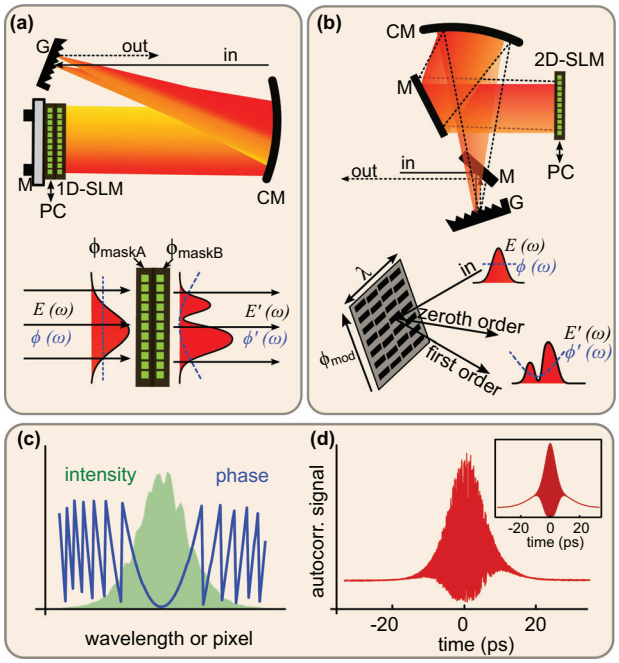

Figure 6. Chirped pulse preparation via SLM using a) transmissive, one-dimensional SLM (1D-SLM), arranged in non-Littrow configuration and b) diffractive, two-dimensional SLM (2D-SLM) designed in Littrow configuration. Illustrative sketches on their working principles are displayed along with. Incoming and outgoing laser beam paths are indicated. In (b), for clarity, the diffractive beam path is indicated by dashed lines. c) An illustrative line-cut of the 2D-phase mask projected on a 2D-SLM for imparting GDD ≈ 10 ps^2. d) Temporal profile of the resultant, chirped pulse as evidenced by its interferometric autocorrelation trace. The simulated trace corresponding to such a chirped pulse profile is enclosed in the inset. G-grating, CM-concave (for 1D-SLM) or cylindrical (for 2D-SLM) focussing mirror, M- flat mirror.

For reliable experiments, one must ensure a smooth phase variation across the discrete SLM pixels. It is advantageous to work in the phase wrapping range between -π and π for reduced voltage variation and therefore minimized crosstalk between pixels. In the case of 1D-SLM used for phase-amplitude shaping scattered light from non-addressed pixels contributes to the noise, which could affect the purity of the generated photons, unless a strict filtering is implemented. In the case of 2D-SLM, where the non-addressed pixels do not diffract light in the same direction as the diffracted (i.e., shaped waveform), this would not be an issue.

In an SLM-equipped pulse shaper, one must take care to optimize frequency resolution without introducing deleterious effects. The spectral resolution, that is, the smallest resolvable feature in the frequency domain, is an interplay of the input beam size on the grating, the grating period, the focal length of the focusing element, and the minimum pixel size of the SLM. This in turn leads to a finite time window, giving an upper bound for the intensity FWHM of the shaped pulse in a pulse shaper.[6,93,107] For a given SLM pixel number and size, there is an intrinsic trade-off between these: the higher the spectral resolution, the shorter the time window, and the shorter the maximum pulse duration that can be achieved.

Assuming a linear dispersion of the diffraction grating, the position of a single frequency component ω_k at the Fourier plane is given by $X_k = \alpha\omega_k$, where

$$\alpha = \frac{\lambda_0^2 f}{2\pi c d \cos\theta_d} \tag{9}$$

is defined by the parameters of the 4f shaper, f being the focal length of the focusing element, d the grating period, λ_0 the central wavelength, θ_d the diffraction angle of the grating, and c the speed of light. The spot size of a single frequency component at the Fourier plane is given by ref. [6]

$$\Delta x_0 = 2\ln(2)\frac{\cos\theta_i}{\cos\theta_d}\frac{f\lambda_0}{\pi\Delta x_{\text{in}}} \tag{10}$$

where Δx_{in} is the spot size at the grating plane and θ_i is the angle of incidence. Using these two equations, the frequency resolution at the Fourier plane is obtained as

$$\delta\omega = \Delta x_0/\alpha \tag{11}$$

From Fourier relations, the maximum width of the temporal window can be determined as

$$\Delta T = 4\ln(2)/\delta\omega \tag{12}$$

which limits the achievable duration of the chirped pulse. From this, it is clear that the optimal resolution is determined by the input beam size, the period of the grating, and the ratio $\cos\theta_i/\cos\theta_d$.

From Equation (11), it is clear that by using a larger input beam one can achieve an enhanced resolution limit, however it introduces beam distortion and spatiotemporal coupling (for detailed analysis, see refs. [120–126]). Such artifacts have an important effect on multiphoton quantum control experiments.[40,73,127,128] For instance, the spatial overlap of different colours in the laser spectrum can be significantly altered. The modified electric field seen by the quantum emitter in the excitation volume,[72,125,129] can result in inefficient excitation. Additionally, optical aberrations can also reduce the single-mode fiber coupling of the shaped laser pulses. Therefore, the spatio-spectro-temporal features on the excitation spot must be carefully characterized. For experiments using broadband laser pulses, to ensure accuracy in the imparted phase profiles, careful phase compensation routines need to be performed.[130,131] Another way to mitigate spatio-temporal coupling artifacts is to opt for a double passed ($2\times 4f$ = $8f$) shaper as discussed in ref. [129]; however, at the cost of lower efficiency. Therefore, depending on the complexity of the spatio-temporal waveform generated and the requirements of the experiment, appropriate measures have to be taken. A summary of SLM-based pulse shaping is presented in **Table 3**.

Example Design 1: Consider a 4f pulse shaper equipped with an SLM arranged in Littrow-configuration (see Figure 6b), coupled to a laser source centered at 795 nm with a transform-limited pulse duration of 1.7 ps. The intensity spectrum of this laser spans from 794.2 nm to 795.8 nm (assuming 3x intensity FWHM). Employing a 1800 groove/mm grating (Littrow angle ≈ 46°), and a 500 mm focal length concave mirror (or lens), for

Table 3. Summary of the advantages and disadvantages of spatial light modulator-based chirping implementations.

SLM-based chirping	
Advantages	Disadvantages
• Adaptive and programmable spectral phase control, including higher-order components • Can generate complex waveforms with arbitrary polarizations • Imparting negative dispersion does not increase the footprint as in grating stretchers • Customizable for arbitrary wavelengths	• Electronically non-addressed areas contribute to noise • Spatiotemporal couplings present • Throughput depends on the grating efficiency • Limited dispersion range • Slow response time • Requires active cooling for higher power level

an input spot size of 2.5 mm, this configuration achieves a single wavelength beam diameter of 70.2 μm at the Fourier plane, and the width of the spectrum will span 2.1 mm at the Fourier plane. The frequency resolution of such a system is 0.162 THz (0.34 nm), and from Equation (12), the resulting time window is 17.1 ps. From this, the maximum chirp that can be applied is 10.4 ps^2. For reference, the typical pixel size for an LCOS-SLM is 10 μm, meaning that 0.162 THz frequency bin is spread across ≈ 7 pixels. Note that, going for a smaller spot size at the SLM plane to match the pixel size might not be advantageous, as one might face issues like inter-pixel crosstalk.[132]

Example Design 2: The design of an SLM-based pulse shaper must be tailored to the laser system associated with it. Consider a laser source with a center wavelength of 1300 nm, and a transform-limited pulse duration of 125 fs. The spectrum of this laser source spans 60 nm from 1270 nm to 1330 nm. Because of larger bandwidth of this laser, a grating with a smaller number of grooves (i.e., larger period) should be used to prevent over-filling the SLM. For example, with a 600 groove/mm grating (Littrow angle ≈ 23°) and a 500 mm focal length focusing mirror, the resulting spot size at the Fourier plane is 114 μm. Using this design, the frequency resolution is 0.39 THz (2.2 nm), which leads to a time window of 7.06 ps, meaning the maximum chirp that can be applied is 0.32 ps^2.

It is therefore clear that the Design 1 is sub-optimal for chirped *two-photon excitation* of a quantum dot at 800 nm (see Figure 3a–c), where the required GDD is ≈ 45 ps^2.[40,53] On the other hand, the Design 2 satisfies the requirements of the chirped *p-shell excitation* (see Figure 3d–f) where the GDD requirement is within the SLM capabilities.[38,54]

Interestingly, one can expand the GDD limit by choosing a non-Littrow configuration for the pulse shaper. For instance, in Design 1, using the same grating and the focussing element, with an incident angle of 67°, the time window becomes 30 ps, allowing for a higher chirp of 18 ps^2. Note that this is still insufficient for chirped *two-photon excitation* (see Figure 3a–c).

Efficiency: The total efficiency of SLM-based chirping depends on grating efficiency $\eta_{grating}$ and the SLM efficiency. Assume that the liquid crystal transmission efficiency is η_{trans}. For simultaneous phase-amplitude shaping with a 1D-SLM, one requires a dual mask configuration. When operated in a folded, double-pass configuration, the total power throughput is then

$$\eta_{1DSLM} = \eta_{trans}^4 \cdot \eta_{grating}^2 \tag{13}$$

For $\eta_{grating}$ = 70% at 795 nm, and a typical liquid crystal transmission efficiency η_{LC} = 80% (ref. [133]), the total efficiency will be only 15%.

On the other hand, the total efficiency of diffractive SLMs is

$$\eta_{2DSLM} = \eta_{ref} \cdot \eta_{diff} \cdot \eta_{grating}^2 \tag{14}$$

where the first two terms refer to the reflection and diffraction efficiencies, respectively, of the SLM. According to the specifications of optimized designs at 800 nm, η_{diff} and η_{ref} are in the range of 70% and 97%, respectively.[134] This brings the total efficiency to around 33%. In both cases, additional losses can arise from output fiber coupling and polarization optics.

Outlook: Most of the commercial 1D-SLMs have pixel sizes on the order of 98 μm, while for the 2D-SLMs they are on the order of 10 μm. That said, in refs. [135, 136], the authors utilized a custom-designed SLM with pixel size 1 μm and a total of 12,288 pixels to demonstrate a high-resolution, arbitrary phase-amplitude shaping. However, developmental costs for such customized designs are huge, and extreme care has to be taken to minimize crosstalk between pixels. In another recent development, some works have explored the use of virtually imaged phase arrays[137–139] or tilted chirped volume Bragg gratings[140] instead of diffraction gratings in a 4*f* shaper, in combination with SLM, for specific purposes.

Another important aspect of SLM-based pulse shaping is the modulation speed, which are typically on the kHz range. Modern implementations, however, provide better and faster modulation.[141,142] Inspiring recent developments show that, SLM or similar active modulation devices, together with tailored metasurfaces[143–145] can bring novel routes in arbitrary spatiotemporal control of quantum light.

4.3. Chirped Fiber Bragg Gratings

So far in this article, we have discussed the techniques to provide controllable chirp values. In certain occasions (for details see Section 6), one only needs a fixed, high chirp value. In the remaining part, we describe two such methods.

Chirped fiber Bragg gratings (CFBGs) are fiber-integrated solutions for producing chirped pulses.[146] Contrary to the methods discussed so far in this article, with CFBGs, one does not need a 4*f* pulse shaper. Here instead, an optical fiber core is imparted with a periodic variation of the refractive index. In the simplest case, as presented in **Figure 7a**, when the period of refractive index modification is constant, we obtain a narrowband reflection corresponding to the Bragg resonance, that is, a narrowband frequency filter called a fiber Bragg grating (FBG). These are commonly used as narrowband frequency filters. One can also, however, generate a linearly varying period of the refractive index modification along the propagation direction *z* (i.e., controlling the Bragg reflection resonances at various positions). In this case, different wavelengths are reflected at different spatial

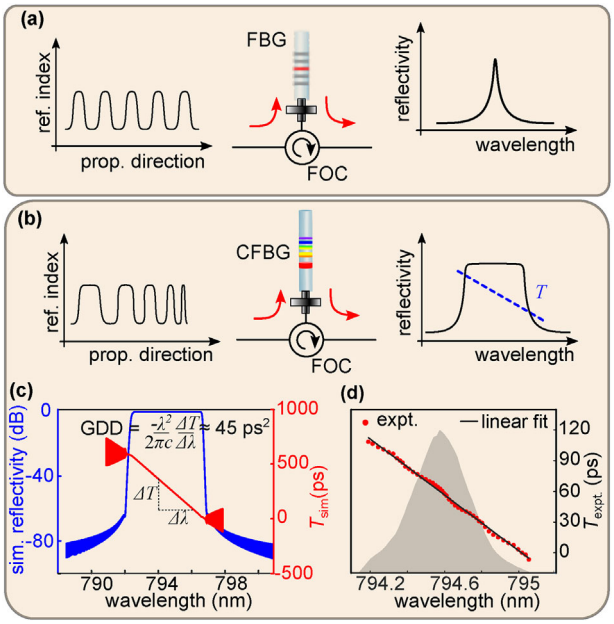

Figure 7. Pulse chirping using tailored fiber Bragg gratings: a) Working principle of a regular fiber Bragg grating (FBG), in comparison with b) chirped fiber Bragg gratings (CFBG). For CFBG, the propagation direction indicated is for GDD > 0. A fiber-optic circulator (FOC) helps separate the incoming and outgoing beams. *T*- wavelength-dependent time delay (c.f. Figure 1). c) Simulated reflection spectrum (blue curve) of the CFBG designed for ±45 ps^2 chirp, centered at 794.5 nm and simulated time delay (*T*, red curve) of different wavelengths. The negative slope of the red curve determines the dispersion parameter $D_{1\lambda}$, from which the GDD is computed, as indicated in the formula. d) CFBG dispersion measurement: measured time delays (*T*) of different wavelengths via a time-of-arrival technique. Red dots denote the peak wavelengths recorded in the +45 ps^2 direction and the black line denotes the fit. The slope of the solid black line provides the dispersion parameter $D_{1\lambda}$. Grey shade represents the laser spectrum. (c) and (d) adapted with permission.[53] Licensed under a Creative Commons Attribution (CC BY) license 2023.

positions in the fiber core along the propagation direction. This results in a wavelength-dependent path length difference, which corresponds to the chirp. The working principle of a CFBG is sketched in Figure 7b. Note that in the case of grating stretchers, the path length difference between various wavelengths is obtained by angular dispersion, which inherently imposes spatiotemporal coupling, while in CFBGs, angular dispersion is absent.

The reflected wavelength λ_B depends on the grating period Λ and the effective refractive index n_{eff} of the guided mode in the fiber core by $\lambda_B(z) = 2n_{eff}(z)\Lambda(z)$. To calculate the spectral response of the designed CFBG parameters and to determine the required linear period variation, that is, the chirp rate of the CFBG, one can utilize the transfer matrix algorithm as described in ref. [147]. In Figure 7c, we present the simulated reflectivity and dispersion characteristics of a CFBG designed at 794 nm to provide 45 ps^2 chirp. It is clear that the propagation direction in a CFBG dictates the sign of chirp. The refractive index modulation can be designed for a reasonably high second or even higher-order phase modulation.

CFBGs were primarily developed for dispersion compensation in optical communication systems.[148,149] Later, they became phenomenal in the development of compact short-pulse fiber laser sources with high peak powers,[150,151] relying on the technique of chirped pulse amplification.[22] Subsequently, they found applications in fiber-optic sensing,[152–155] high time resolution spectroscopy,[156,157] advanced signal processing applications[26,27] and pulse shaping schemes.[158–161] With CFBGs, by cascading several of them,[159] one can obtain a wide range of GDDs without drastically increasing the complexity of the setup.

In the case of quantum dot technologies, CFBGs have a huge potential.[53] In recent years, considerable effort has been invested in the development of a plug-and-play, direct fiber-coupled source.[162–166] To ensure a long-term stable quantum light source operated in a leave-and-forget mode, a simple yet robust excitation scheme is preferred. Given this context, the CFBGs enable one to exploit all the advantages of coherent, chirped excitation methods. As CFBGs provide an aberration-free, single-mode fiber-based chirping mechanism, the challenges encountered in other methods do not matter, that is, beam distortions and spatiotemporal artifacts are absent. Although it operates with a fixed spectral bandwidth, it can be matched well with the typical spectral variability of quantum dots ≈10 nm.[44,45] As a compact and alignment-free technique, it is also unaffected by the mechanical vibrations of the optical table.

Recently, we have fabricated CFBGs at ≈794 nm to match the resonance of GaAs/AlGaAs quantum dots (see Figure 7c) and demonstrated high-efficiency chirped *two-photon excitation* of a single quantum dot.[53] The measured dispersion (for details see Section 5) and reflectivity, presented in Figure 7d match well with the design parameters. The CFBGs were fabricated via a femtosecond phase mask inscription method (for more details on the fabrication, see ref. [146]). The versatility of CFBGs allows directly coupling the chirped pulses to the quantum dot, enabling a truly robust and long-term stable quantum light source.

Practical Considerations: A CFBG has to be designed for each specific use case. The achievable GDD depends on the bandwidth $\Delta\lambda$ and the maximum possible length of the CFBG L_{CFBG} as well as the target wavelength λ_0, which can be approximated by

$$\mathrm{GDD} \approx \frac{n}{\pi c^2}\frac{\lambda_0^2 L_{\mathrm{CFBG}}}{\Delta\lambda} \tag{15}$$

Typical grating lengths are in the range of a few millimeters up to 15 cm. Given this, one can achieve a GDD of 45 ps^2 with a bandwidth > 10 nm at 900 nm or > 35 nm at 1550 nm central wavelength. However, with more complex inscription approaches, ultralong gratings ($L_{CFBG} \approx 1$ m) have been demonstrated.[167]

The quality of the CFBG inscription and design of the refractive index modulation along the fiber is an important aspect, as noise or deviations along the propagation direction lead to amplitude and phase ripples on the spectral response, which can cause pulse distortions.[168] Also, an inhomogeneous refractive index modulation can lead to wavelength-dependent losses resulting from cladding mode coupling.[146]

The spectral resonance of a CFBG is sensitive to its surrounding temperature as well as to applied strain on the fiber.[169] Any change in the refractive index, or the compression/dilation of

Table 4. Summary of the advantages and disadvantages of chirping methods based on chirped fiber Bragg gratings.

CFBG-based chirping	
Advantages	Disadvantages
• Spatiotemporal couplings absent • Compact, alignment-free and fully-fiber based plug-and-play device • Can be engineered for arbitrary phase profiles • Cascaded operation possible • Dispersion tunable	• Design-specific use • Throughput depends on the circulator efficiency

the grating causes a shift of the resonance wavelength, grating chirp, and consequently the dispersive response of the CFBG. Therefore, they must either be thermally and mechanically protected or placed in an athermal packaging where small temperature changes can be compensated by compressing or dilating the grating. In fact, these features can be exploited to achieve a desired tunability, for example, to match a specific resonance by a few hundred picometers even up to nanometers depending on the fiber type and wavelength range. By applying a temperature gradient along the grating, one can also adapt the GDD.[170] Note that in fibers, the laser power and propagating length must be adjusted to avoid other nonlinear effects like self phase modulation,[171] which introduces spectral variation and nonlinear chirps.[172] For quantum dot experiments, however, the laser power used is considerably low. Specifically, in ref. [53], the average laser power was <650 μW (with pulse duration 2 ps and 80 MHz repetition rate, the peak power will be ≈ 4 W), and therefore laser-induced nonlinearities are not expected to play a role. The important features of the CFBG-based chirping scheme are presented in **Table 4**.

Efficiency: Assuming a fiber-coupled laser source, the maximum efficiency in CFBG-based chirping is

$$\eta_{\mathrm{CFBG}} = \eta_{\mathrm{FOC}}^2 \cdot \eta_{\mathrm{ref}} \tag{16}$$

where η_{FOC} is the efficiency of the fiber-optic circulator (where the light undergoes double pass, and therefore η_{FOC}^2) and η_{ref} consists of the reflective (and possibly scattering) efficiency of the CFBG.[173] In our experiments, the characterized efficiencies were $\eta_{\mathrm{FOC}}^2 = 77\%$, and $\eta_{\mathrm{ref}} = 90\%$. However, the measured total efficiency was 40%, [53] with the remaining losses attributed to fiber mating inefficiencies. In a practical application, one could mitigate this by splicing the CFBG ends to the circulator.

4.4. Chirped Volume Bragg Gratings

Similar to CFBGs, the refractive index variation required to generate wavelength-dependent path length delay difference can also be engineered in a bulk material. This is precisely the working principle of chirped volume Bragg gratings (CVBG),[174–176] illustrated in **Figure 8a**. They are produced by holographic recording on a piece of photo-thermo-refractive glass, and can be tailored for a wide range of operation wavelengths. Note that CVBGs are different from the chirped mirrors[81,82] as the refractive index

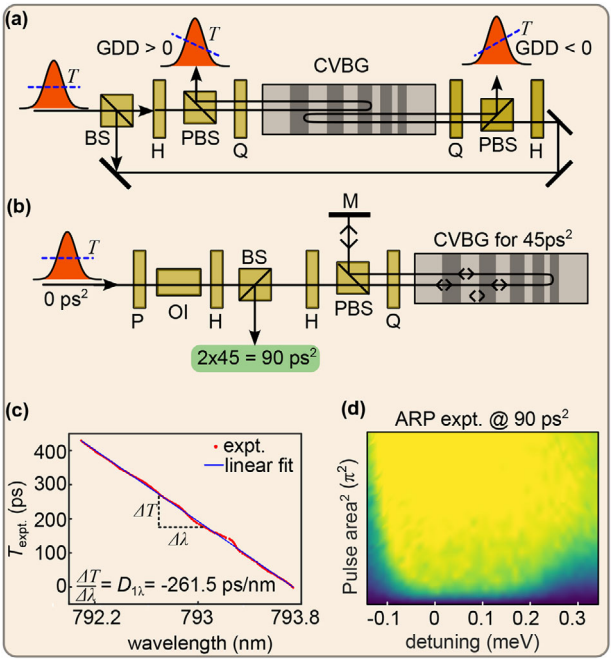

Figure 8. Chirped pulse preparation using chirped volume Bragg gratings (CVBG): a) Simultaneous preparation of positively and negatively chirped pulses (GDD = ±45 ps²) using the CVBG. A 50:50 beamsplitter (BS) splits the incoming laser beam into two, one for positive chirp and the other for negative chirp. Incoming and chirped laser pulses are separated via polarization filtering, relying on the combination of a half-wave plate (H), a polarizing beamsplitter (PBS), and a quarter-wave plate (Q). b) Demonstration of additive dispersion: the 45 ps² pulses are retroreflected back to the CVBG to double the GDD. The incoming (GDD = 0 ps²) pulses and the outgoing (GDD = 90 ps²) pulses are separated via the combination of a polarizer (P), (Faraday) optical isolator (OI) and a half-wave plate (H). c) Experimental confirmation of the generation of GDD = 90 ps² pulses via the time-of-arrival method (see Figures 7d and 9d), with the computed slope displayed along with. d) Demonstration of ARP excitation using 90 ps² pulses.

modification in the former is much smaller and spreads over longer material length, which gives the possibility to generate high values of chirp. In contrast to CFBGs, the propagating beam inside a CVBG is unguided. As a result, the reflected, frequency-chirped beam from a CVBG might experience a non-negligible spatial chirp as well.[140] Nevertheless, it is easy to align, and as illustrated in Figure 8a, one can simultaneously obtain both positively and negatively chirped pulses from a single element.

In a CFBG, the transverse aperture size is limited by the maximum achievable single-mode core size ≈ 8 μm, while that of a CVBG is limited only by the grating writing technology. For PTR glass technology, this can potentially be several millimeters.[177] Similar to CFBGs, the reflection bandwidth of a few 10 s of nanometers is possible for CVBGs too. An important advantage is that CVBGs handle average powers of several watts,[178] have polarization-independent efficiency, and are resistive to shocks and vibrations. In contrast to CFBGs, the circulator efficiency is also not a concern here, if one chooses to operate in the configuration illustrated in Figure 8a. Interestingly, novel designs like rotated CVBGs designed to reflect the resonant wavelengths from side facets[179] can be combined with programmable elements

like spatial light modulators[140] to achieve diverse and complex pulse shaping methods.

Interestingly, CVBGs allow multiple passes on a single element, thereby allowing GDD multiplication. An example is illustrated in Figure 8b, employing a CVBG (Optigrate), designed for 45 ps^2 at 793 nm. Using a mirror placed at the (positive) output port in Figure 8a, the positively chirped pulses are reflected back to the CVBG, which undergo dispersion yet another time, yielding a GDD of 2×45 ps^2 = 90 ps^2. To prevent the back-propagating beam from re-entering the laser cavity, one must use an optical isolator.

To demonstrate the versatility of CVBGs, we have measured the wavelength-dependent time delay via the time-of-arrival method (see Section 5 for details), and obtained a $D_{1\lambda} = -262$ ps nm^{-1}, corresponding to a GDD = 88 ps^2, which fits well with the expected GDD = 90 ps^2. We attribute the disparities to other sources of dispersion such as the 4*f* shaper utilized for spectral slicing, the optical isolator, and the spatial chirp and tolerances introduced by the CVBG itself. Furthermore, in Figure 8d we present the results of the *two-photon* ARP experiment on a quantum dot at GDD = 90 ps^2. It is clear that the trend in Figure 3a–c is retained. An interesting advantage of extremely high positive chirp is that it allows the use of narrowband laser pulses for chirped excitation, for instance, in quantum dots with smaller biexciton binding energy (for details see ref. [40]). To the best of our knowledge, this demonstrates the ARP experiment on quantum dots with the largest GDD value reported.

5. Pulse Characterization Methods

One of the major areas of concern for pulse shaping experiments on nanoscale emitters like quantum dots is the precise knowledge and control of spectral phase and amplitude at the microscopic interaction volume. In most circumstances, laser pulses propagate through an arbitrary set of optical elements like beamsplitters, lenses, optical fibers, and objectives which eventually focuses the pulses on the emitter. Such dispersive elements stretch the laser pulse from its Fourier limit by adding dispersion (see Figure 4). Even though for chirped excitation of quantum dots based on the ARP protocol the population inversion is ensured for a range of dispersions above a threshold, on certain occasions, at least an indirect knowledge of the chirp rate is desirable.

Autocorrelation: It is known that nonlinear optical processes like second harmonic generation (SHG) or two-photon absorption have a direct dependence on laser pulse duration.[180,181] Based on this, naively speaking, one can estimate the pulse duration of a chirped pulse, provided the SHG intensity measured with a reference (transform-limited) pulse is available. The most popular approach for pulse duration measurement is intensity autocorrelation,[182] where the interference of two time-delayed laser pulses enables the direct extraction of the laser pulse duration. In ref. [39] reporting chirped excitation of a quantum dot, the authors relied on this method to record the pulse durations at various positions of their grating stretcher, from which the corresponding GDDs were estimated. However, at low power levels, the SHG efficiency is also low, implying that this technique may not be optimal for GDDs > 15 ps^2. In such cases, one may replace the SHG crystal with a two-photon absorbing photodiode to perform fringe-resolved autocorrelation, as demonstrated in refs. [183, 184]. An illustrative sketch of this method is presented in **Figure 9**a. Using this technique, one can extract the properties of laser pulses at energies as low as a few pJ. Based on the measured laser spectrum, and a phase-retrieval algorithm, this technique can be used to fully reconstruct the pulse information with high accuracy,[185,186] depending on the practical necessity. Several other methods have been developed for the complete characterization of laser pulses, like frequency-resolved optical gating[187] and its variations,[188–190] or spectral phase interferometry for direct electric-field reconstruction,[191] and other related methods.[192]

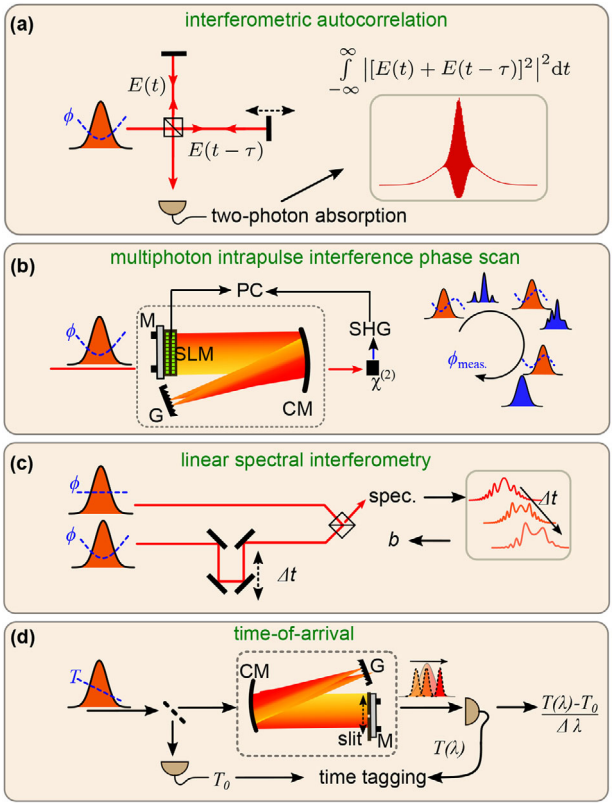

Figure 9. Pulse characterization methods: Sketches of a) Interferometric autocorrelation method with a two-photon absorbing photodiode, b) Multiphoton intrapulse interference phase scan method, c) Linear spectral interference method, and d) Time-of-arrival method, respectively utilized for qualitative estimation of pulse duration, spectral phase characterization and compensation, chirp rate, and the dispersion parameter. M-mirror, G-grating, SLM- spatial light modulator, CM- concave mirror.

Multiphoton Intrapulse Interference Phase Scan (MIIPS): It is important to note that all of the pulse characterization methods described before only allow the measurement of the laser spectral phase and not the subsequent correction. Specifically in the case of chirped excitation using SLM and a broadband pulse,[38,54,109] the imparted GDD to achieve the ARP threshold is accurately known only if one starts with a transform-limited pulse. As femtosecond pulses acquire phase distortion from other optical elements like the objective, precise knowledge of the laser spectral phase at the interaction volume is important, such that it can be corrected, after which the required GDD phase function can be applied. In this context, the technique of MIIPS[130,131] holds spe-

cial importance. It has proven to be a robust approach that not only measures but also *compensates* for the phase distortion utilizing the same SLM-equipped 4*f* shaper, without the need for any additional setup. The working principle of the MIIPS routine is sketched in Figure 9b. In ref. [38] where the authors utilized 120 fs pulses for the ARP protocol, the phase distortion at the sample volume was emulated via an additional objective in a separate optical path, where the phase measurement and compensation are performed using MIIPS. Note that such a procedure can also be performed directly at the interaction volume, provided that one utilizes the nonlinear signal from a reference nanostructure on the same sample.[131]

Linear Spectral Interferometry: As mentioned earlier, despite its advantages, the nonlinear pulse characterization methods are hardly useful at low power levels. For instance, in experiments involving CFBGs,[53] the employed fiber optic circulator had a peak power threshold of 5 W, which is insufficient for generating enough nonlinear signal. For example, with an average power of 750 μW of 2 ps pulses with 80 MHz repetition rate, the peak power is 4.5 W, close to the damage threshold of the fiber optic circulator. Therefore, one has to resort to low-power pulse characterization techniques.

Several methods of linear pulse characterization have been reported in the literature.[193–197] Here, a reference pulse whose temporal properties are known (usually the transform-limited pulses from the laser source) interferes with the chirped pulse at various time delays, while the corresponding spectra are recorded (see Figure 9c). By tracing the asymmetric fringes in the spectral interference patterns corresponding to various time delays, one can derive the chirp rate b (see Equation (12)). A major feature of this technique is that, contrary to the SHG-based method, the accuracy in determining the pulse width is higher as the ratio $\frac{\tau_p}{\tau_0}$ grows, which makes it more suitable for measuring highly chirped pulses as in refs. [40, 53, 91].

Time-of-Arrival: Yet another approach is to measure the laser pulse dispersion directly in the time domain, provided the temporal resolution of the detectors allow it. Consider a chirped pulse (i.e., temporally stretched), where one measures the arrival time $T(\lambda)$ of wavelengths with respect to a reference. In Figure 9d, we illustrate the working principle of this method. Initially, a reference laser pulse is set up as T_0. As the chirped pulse that needs to be characterized, maintains the same intensity spectrum as the transform-limited pulse but is stretched in time, one can rely on detectors with sufficiently low time jitter to estimate the arrival time of individual wavelength components, using a time-tagging device. To choose individual wavelengths, one can utilize either a continuously tunable narrowband filter or, in ref. [53], an automated 4*f* shaper. This way, the arrival times of individual wavelengths (T_λ) composing the chirped pulse are directly recorded in reference to T_0. As a result, one can *directly* obtain $(T_\lambda - T_0)/\Delta\lambda = D_{1\lambda}$ (see Equation (4)) which is the dispersion parameter. In ref. [53], we utilized this technique to estimate $D_{1\lambda}$ of ≈ 45 ps^2 pulses at extremely low powers.

6. Applications

Apart from the existing state-of-the-art, chirped pulse excitation offers further possibilities for quantum dot research and the development of new technologies in the future. In the following section, we describe a few.

6.1. Robust Photon Sources at Engineered Wavelengths

In semiconductor quantum dots-based quantum communication technologies, the focus is on producing bright sources of high-purity single photons and high-fidelity entangled photon pairs, which are the building blocks to realize high-security quantum communication devices. Addressing the scalability aspect, in a realistic scenario, the quantum dot growth processes always introduce intrinsic variability in their properties. Historically, attention was given to developing *identical*, indistinguishable single photons from *different* sources. This meant that having different spectral properties for different quantum dots made it difficult to envision scalable hardware based on quantum dots. Examples are protocols such as teleportation and entanglement swapping[198] used in quantum repeaters as well as photonic-based quantum simulation. However, for certain applications like quantum key distribution based on the BB84 protocol,[199] frequency-multiplexed single photons are desirable, thereby enabling simultaneous key-sharing with multiple participants. The coherent, and simultaneous generation of frequency-multiplexed photons from a quantum dot ensemble offers one the possibility to frequency-convert some of them to different wavelength(s),[200–202] and demonstrate quantum interference.[203,204] Inspiring recent developments[205,206] show that one might be able to utilize nanoscale nonlinear conversion platforms for this. In the future, one can target a single, multifunctional nanoscale resource that can satisfy all the quantum photonic application scenarios. Going hand-in-hand with the advancements in growth processes,[207] frequency-multiplexed sources developed in semiconductor quantum dots[208] can be very well utilized for this purpose.

As illustrated in **Figure 10**, with a CFBG directly coupled to an integrated quantum dot source, the dream of a practical, robust photon source performing against laser power fluctuations or other instabilities, advances closer to reality. Such a stable photon source would allow long-term multiphoton experiments, and for instance in the future, to demonstrate boson sampling with quantum dot photon sources, extending the initial works performed with resonant excitation[209] or quasi-resonant excitation.[210] Additionally, for entanglement-based quantum cryptography,[33,211,212] a stable photon source could be valuable.

6.2. Compact and High-Repetition-Rate Laser Sources for Quantum Communication

High repetition rate laser sources are key to many applications. State-of-the-art diode-pumped solid-state laser sources (for instance Ti: Sapphire) operate at <100 MHz repetition rate and are bulky and expensive. This limits the use of such lasers in practical applications. For instance, as described in Figure 10, consider a frequency-multiplexed quantum dot source driven by a Ti:Sapphire laser source. The photon generation rate from a quantum dot can be enhanced by exploiting the Purcell effect, by embedding the quantum dot in a photonic cavity. This essentially shortens the lifetime of the quantum dot state, that

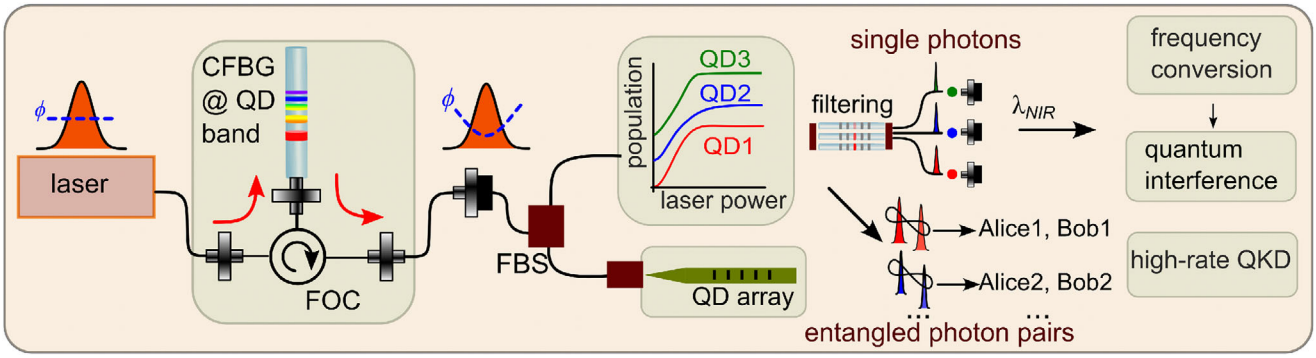

Figure 10. Robust and multipurpose photon source based on a quantum dot ensemble: A compact, high-repetition-rate laser source is coupled to a chirped fiber Bragg grating (CFBG). The CFBG is tailored to generate chirped pulses that coincide with the quantum dot spectral window and is directly coupled to the quantum dot source via a fiber beamsplitter (FBS). Relying on the process of adiabatic rapid passage, the quantum dot ensemble is excited efficiently and produces single (or entangled) photon states. These frequency-multiplexed photons are collected via the same fiber and are filtered to separate applications like frequency conversion, high-rate quantum key distribution (QKD), and so on.

is, the number of possible optical excitation-emission cycles within a given time window is increased. However, this reaches a limit, ultimately dictated by the repetition rate of the laser source. In this context, one could take advantage of FBGs and CFBGs,[213] to achieve compact, efficient, and high repetition rate laser sources with engineered pulse characteristics. Such a compact laser would replace the bulky Ti:Sapphire laser, and bring the dream of a truly plug-and-play quantum dot photon source[162] closer to reality than ever.

The vast potential of pulse shaping techniques could be, in principle, extended further in the direction of ARP scheme.[109,214] For instance to realize entangled photon states from non-degenerate and spatially distinct quantum dots as theoretically proposed in ref. [75]. In a recent novelty, in ref. [73], the authors used a broadband laser pulse and implemented phase-amplitude shaping to create a spectral notch on the targeted exciton line and chirped the pulse to achieve high-efficiency preparation of the exciton state. It would be interesting to explore the potential of this technique in the case of a quantum dot ensemble. In the future, with quantum dot sources integrated into tailored photonic cavities,[215] one could explore cooperative interactions in different coupling regimes as well.

6.3. Advanced Superresolution Imaging

Quantum dots are one of the most important labeling agents for super-resolution fluorescence imaging.[216,217] Popular methods of superresolution imaging are either stochastic localization-based,[218,219] fluorescence-fluctuation (blinking) based,[220] excitation laser modulation based,[221] or point spread function engineering based.[222–224] The last one utilizes a combination of Gaussian and doughnut (spatially shaped) laser beams to shrink the microscopic point spread function. All of these techniques are incoherent, that is, the excited states in the emitter lose the phase memory with respect to the excitation source or have the disadvantage of using multiple laser sources.

In a historic achievement, coherent nanoscopic imaging was demonstrated, relying on the scheme of Rabi oscillations[225] in molecular systems at cryogenic temperatures. However, due to the sensitivity of Rabi scheme to the pulse area, the fluorescence image of an emitter appears as a series of concentric circles. Beyond the preservation of phase memory, the Rabi scheme therefore has limitations in being used as a truly coherent superresolving imaging technique. Recently, in ref. [71] the authors demonstrated a robust on-off switching technique, employing a pair of chirped laser pulses of opposite sign that is also spatially shaped as in conventional superresolution techniques, and achieved the shrinking of the point spread function. In **Figure 11**, we sketch the concept. Note that in the original work, the authors employed two separate grating stretchers, each set for positive and negative dispersions, respectively. However, using a CVBG, which offers positive and negative chirps with a compact monolithic element (c.f. Figures 8b and 11a) might widen the scope of the technique. The resultant dispersed pulses are directed to the QD sample to perform a scanning confocal or widefield excitation. Note that, akin to the stimulated emission depletion (STED) approach, positively chirped pulses are designed as Gaussian-shaped, and negatively chirped pulses are doughnut-shaped (Figure 11b). For the latter, one can employ phase plates (as in the original work[71]), or an SLM.[226] Using an SLM provides one with a wide range of possibilities, for instance, to generate beams with vectorial properties,[227] and/or with simultaneous phase-amplitude shaping. Following the beam shaping stage, the positively chirped pulses, acting as the ON pulses, bring the QD ensemble to their excited states, relying on ARP. The negatively chirped pulses, act as depleting (i.e., OFF) pulses, bringing the population back to the ground state (Figure 11c). The eventual result is that the point spread function based on the QD emission is shrunk, providing the necessary improvement in spatial resolution (Figure 11d). Note that in ref. [71], the authors demonstrated the technique by targeting the exciton state, which demands stringent cross-polarization filtering[228] because the laser energy is resonant with the exciton energy. Alternatively, one could use two-photon excitation ARP targeting the biexciton state[39,40] and rely on simple spectral filtering, and therefore take advantage of a better signal-to-noise ratio. With rapidly evolving illumination engineering methods,[226,229] a robust imaging scheme for a large ensemble of quantum dots is within reach. In the future, with the improved performance of quantum dots at ambient tempera-

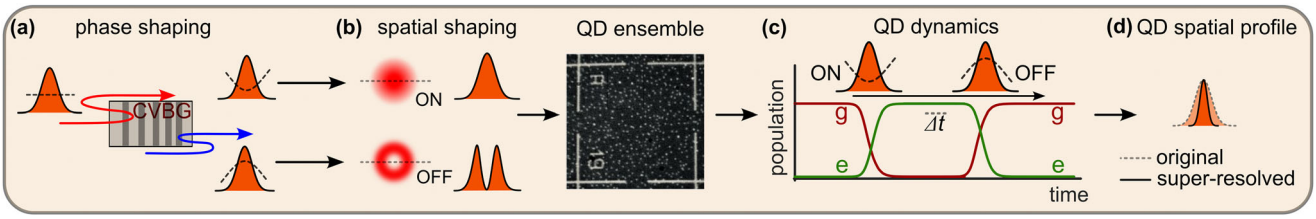

Figure 11. Coherent superresolution imaging enabled by ARP, as proposed in ref. [71]: a) Initially, positively- and negatively-chirped pulses are prepared with a suitable chirping method (here, CVBG). b) The positively chirped pulse maintains a Gaussian shape (acting as ON-pulse) while the negatively chirped pulse is spatially shaped to have a doughnut profile (acting as OFF-pulse) with an SLM or a phase plate (not shown). This ON-OFF pulse sequence is directed to a QD ensemble for a raster scan or widefield fluorescence imaging. c) Schematic of the QD population dynamics. The Gaussian-shaped positively chirped pulse induces the ARP process (i.e., fully populate the excited state), while the doughnut-shaped negatively chirped pulse inverts the system back to the ground state, giving rise to the coherent, super-resolved spatial profile sketched in d).

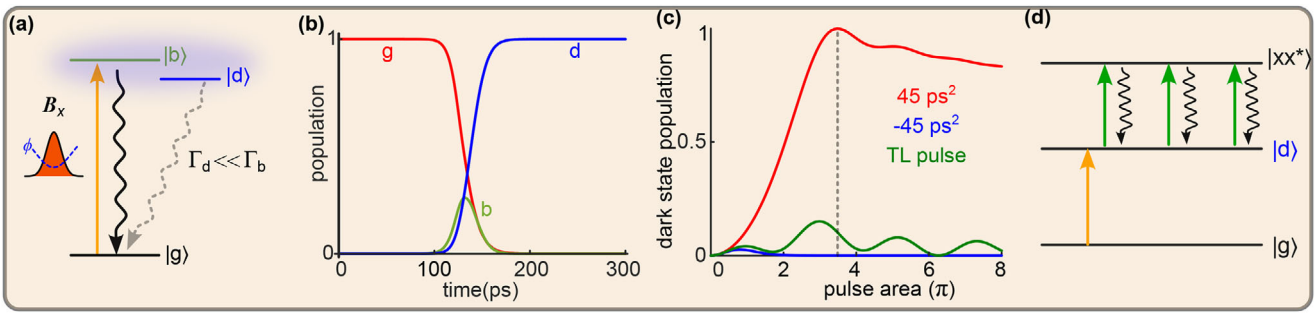

Figure 12. Dark state excitation using chirped pulses, as proposed in Ref. [231]: a) Level scheme of a quantum with the ground (|g⟩), bright exciton (|b⟩) and dark exciton (|d⟩) states. b) Simulated population dynamics of these states under chirped pulse excitation with laser energy close to the resonance |g⟩ ↔ |b⟩ in presence of an in-plane magnetic field. c) Simulated dark state population under a pulse area scan for 45 ps^2, -45 ps^2 and transform-limited (TL) pulse excitations. d) Schematic of the sequence of transitions in a quantum dot required to generate a cluster state relying on the dark state, as proposed in ref. [232]. Quantum dot-specific parameters used in this simulation, including the in-plane g-factors, are taken from a measured data set and are available upon request.

tures, or based on different quantum dot platforms,[230] one could hope for robust and coherent superresolution imaging of biological samples, without the need for multiple laser sources.

6.4. Dark Exciton States

In semiconductor quantum dots, the confinement of carriers and the resultant exchange interaction results in not only bright excitons (described earlier) but also spin-forbidden and therefore optically "dark states" with decay rates orders of magnitude smaller than their bright counterparts ($\Gamma_d \ll \Gamma_b$).[233] In recent years dark states in semiconductor quantum dots[231,234,235] have received increased interest due to their long lifetimes and the possibility of acting as a meta-stable state for quantum information protocols[236] for instance the building of a multi-photon cluster state[232] or as a quantum memory for advanced entanglement schemes,[237,238] and so on. Up until now, the preparation of the dark state in quantum dots has only been realized by relying on radiative and non-radiative decays from higher energy states in quantum dots,[232] electrical injection[234] or spin flip mediated by external magnetic impurities,[239] or by distorting the symmetry in quantum dots.[240] In ref. [231], the authors proposed that by using chirped laser pulses in combination with external magnetic fields (see **Figure 12a**), unwanted decays from the higher excited state can be circumvented and coherently prepare the dark state. This offers a simple and practical implementation of advanced quantum protocols. In Figure 12b we present the population dynamics of a quantum dot system with the dark state (|d⟩) under the influence of an in-plane magnetic field of 4 T and a positively (45 ps^2) chirped laser pulse of 0.2 nm bandwidth that is nearly resonant to the bright exciton (|b⟩). In Figure 12c, we present the simulated dark state population for a pulse-area sweep with ±45 ps^2 and the transform-limited pulses. For a pulse area of $\approx 3.5\pi$, for 45 ps^2, one attains nearly a unity dark state preparation efficiency, while negatively chirped and the transform-limited pulses do not do so efficiently. Having reached the dark state, one could rely on further transitions and decays in the quantum dot system to implement deterministic entanglement protocols, memories, and so on.

7. Conclusions

To summarize, in this article, we have reviewed the concept behind chirped laser pulses and experimental techniques to produce them, by specifically putting the case of quantum dot excitation into the context. Initially, we started with a brief conceptual overview of chirped pulse excitation, by taking the adiabatic rapid passage process in quantum dot as an example, with a summary of the existing achievements in the field. Subsequently, we inspected the technical quirks of selected experimental techniques to produce chirped laser pulses, by weighing in on their advantages and disadvantages, and included a repre-

sentative design example for each case. We have also included a brief overview of the selected methods to characterize chirped laser pulses, exemplifying their practical relevance. Finally, inspired by the recent developments in this interdisciplinary research field, we have envisioned a few illustrative future applications. We expect that considering phenomenal progress in spatio-spectro-temporal beam-shaping techniques, in addition to rapid advancements in nanofabrication methods, chirped pulses have a huge prospect of making a strong impact in the field of quantum dot-based quantum photonic architecture.

Acknowledgements

The authors gratefully acknowledge helpful discussions with Dmitry Pestov (IPG Photonics), Rob Tiernan (Boulder Nonlinear Systems), Ron Stepanek (Meadowlark Optics), Thomas Niedereichholz (Hamamatsu), Nicoló Accanto (INSERM), Matz Liebel (VU Amsterdam), Niek van Hulst (ICFO), Amit Agrawal (NIST), Arunangshu Debnath (DESY), Alexander Jesacher and Stefan Bernet (MU Innsbruck), Stefan Frick (Uni. Innsbruck) and Armando Rastelli (JKU Linz). FK, YK, RS, MK, SG, GW and VR acknowledge financial support through the Austrian Science Fund FWF projects with grant IDs 10.55776/TAI556 (DarkEneT), 10.55776/W1259 (DK-ALM Atoms, Light, and Molecules), 10.55776/FG5, and 10.55776/I4380 (AEQuDot). TKB and DER acknowledge financial support from the German Research Foundation DFG through project 428026575 (AEQuDot). RGK and SN acknowledge financial support from the German Federal Ministry of Education and Research through project 13N16028 (MHLASQU) and the German Research Foundation DFG (455425131, OH-SUPER).

Conflict of Interest

The authors declare no conflict of interest.

Keywords

chirped pulses, entangled photons, quantum dots, single photons

Received: October 10, 2023
Revised: December 19, 2023
Published online: January 9, 2024

[1] W. S. Warren, H. Rabitz, M. Dahleh, *Science* **1993**, *259*, 1581.
[2] D. Goswami, *Phys. Rep.* **2003**, *374*, 385.
[3] Y. Silberberg, *Annu. Rev. Phys. Chem.* **2009**, *60*, 277.
[4] A. Weiner, *Prog. Quantum Electron.* **1995**, *19*, 161.
[5] H. Kawashima, M. M. Wefers, K. A. Nelson, *Annu. Rev. Phys. Chem.* **1995**, *46*, 627.
[6] A. Monmayrant, S. Weber, B. Chatel, *J. Phys. B At. Mol. Opt. Phys.* **2010**, *43*, 103001.
[7] C. Froehly, B. Colombeau, M. Vampouille, *Prog. Opt.* **1983**, *20*, 63.
[8] I. Walmsley, L. Waxer, C. Dorrer, *Rev. Sci. Instrum.* **2001**, *72*, 1.
[9] C. J. Bardeen, Q. Wang, C. V. Shank, *Phys. Rev. Lett.* **1995**, *75*, 3410.
[10] M. Dantus, V. V. Lozovoy, *Chem. Rev.* **2004**, *104*, 1813.
[11] A. Natan, U. Lev, V. S. Prabhudesai, B. D. Bruner, D. Strasser, D. Schwalm, I. Ben-Itzhak, O. Heber, D. Zajfman, Y. Silberberg, *Phys. Rev. A* **2012**, *86*, 043418.
[12] B. Chatel, J. Degert, S. Stock, B. Girard, *Phys. Rev. A* **2003**, *68*, 041402.
[13] G. Cerullo, C. Bardeen, Q. Wang, C. Shank, *Chem. Phys. Lett.* **1996**, *262*, 362.
[14] D. Maas, D. Duncan, R. Vrijen, W. van der Zande, L. Noordam, *Chem. Phys. Lett.* **1998**, *290*, 75.
[15] A. Assion, T. Baumert, J. Helbing, V. Seyfried, G. Gerber, *Chem. Phys. Lett.* **1996**, *259*, 488.
[16] N. V. Vitanov, B. W. Shore, K. Bergmann, *Eur. Phys. J. D* **1998**, *4*, 15.
[17] I. R. Solá, V. S. Malinovsky, B. Y. Chang, J. Santamaria, K. Bergmann, *Phys. Rev. A* **1999**, *59*, 4494.
[18] J. C. Davis, W. S. Warren, *J. Chem. Phys.* **1999**, *110*, 4229.
[19] V. Remesh, G. Grinblat, Y. Li, S. A. Maier, N. F. van Hulst, *ACS Photonics* **2019**, *6*, 2487.
[20] L. Piatkowski, N. Accanto, N. F. van Hulst, *ACS Photonics* **2016**, *3*, 1401.
[21] V. Giegold, K. Kołataj, T. Liedl, A. Hartschuh, *ACS Photonics* **2022**, *9*, 3727.
[22] D. Strickland, G. Mourou, *Opt. Commun.* **1985**, *55*, 447.
[23] G. Mourou, T. Tajima, *Science* **2011**, *331*, 41.
[24] J.-Q. Liao, C. Law, *Phys. Rev. A* **2011**, *84*, 053838.
[25] Y. Kim, D. Y. Kim, *Opt. Express* **2007**, *15*, 16357.
[26] C. E. Cook, *Proc. IRE* **1960**, *48*, 310.
[27] P. J. Delfyett, D. Mandridis, M. U. Piracha, D. Nguyen, K. Kim, S. Lee, *Prog. Quantum Electron.* **2012**, *36*, 475.
[28] E. Louzon, Z. Henis, S. Pecker, Y. Ehrlich, D. Fisher, M. Fraenkel, A. Zigler, *Appl. Phys. Lett.* **2005**, *87*, 241903.
[29] T. Calarco, A. Datta, P. Fedichev, E. Pazy, P. Zoller, *Phys. Rev. A* **2003**, *68*, 012310.
[30] S. Frick, R. Keil, V. Remesh, G. Weihs, *Photonic Quant. Technolog.: Sci. Appl.* **2023**, *1*, 53.
[31] P. Senellart, G. Solomon, A. White, *Nat. Nanotechnol.* **2017**, *12*, 1026.
[32] D. A. Vajner, L. Rickert, T. Gao, K. Kaymazlar, T. Heindel, *Adv. Quantum Technol.* **2022**, *5*, 2100116.
[33] C. Schimpf, M. Reindl, D. Huber, B. Lehner, S. F. C. D. Silva, S. Manna, M. Vyvlecka, P. Walther, A. Rastelli, *Sci. Adv.* **2021**, *7*, eabe8905.
[34] C. M. Simon, T. Belhadj, B. Chatel, T. Amand, P. Renucci, A. Lemaitre, O. Krebs, P. A. Dalgarno, R. J. Warburton, X. Marie, B. Urbaszek, *Phys. Rev. Lett.* **2011**, *106*, 166801.
[35] Y. Wu, I. M. Piper, M. Ediger, P. Brereton, E. R. Schmidgall, P. R. Eastham, M. Hugues, M. Hopkinson, R. T. Phillips, *Phys. Rev. Lett.* **2011**, *106*, 067401.
[36] A. Debnath, C. Meier, B. Chatel, T. Amand, *Phys. Rev. B* **2013**, *88*, 201305.
[37] S. M. Arif, S. Datta, D. Roy, M. Ghosh, *Eur. Phys. J. Plus* **2022**, *137*, 1170.
[38] R. Mathew, E. Dilcher, A. Gamouras, A. Ramachandran, H. Y. S. Yang, S. Freisem, D. Deppe, K. C. Hall, *Phys. Rev. B* **2014**, *90*, 035316.
[39] T. Kaldewey, S. Lüker, A. V. Kuhlmann, S. R. Valentin, A. Ludwig, A. D. Wieck, D. E. Reiter, T. Kuhn, R. J. Warburton, *Phys. Rev. B* **2017**, *95*, 161302.
[40] F. Kappe, Y. Karli, T. K. Bracht, S. F. C. da Silva, T. Seidelmann, V. M. Axt, A. Rastelli, G. Weihs, D. E. Reiter, V. Remesh, *Mater. Quantum Technol.* **2023**, *3*, 025006.
[41] A. J. Ramsay, *Semicond. Sci. Technol.* **2010**, *25*, 103001.
[42] S. Lüker, D. E. Reiter, *Semicond. Sci. Technol.* **2019**, *34*, 063002.
[43] D. Tannor, *Introduction to Quantum Mechanics*, University Science Books, Melville, NY **2007**.
[44] S. F. C. da Silva, G. Undeutsch, B. Lehner, S. Manna, T. M. Krieger, M. Reindl, C. Schimpf, R. Trotta, A. Rastelli, *Appl. Phys. Lett.* **2021**, *119*, 120502.
[45] P. Laferrière, E. Yeung, I. Miron, D. B. Northeast, S. Haffouz, J. Lapointe, M. Korkusinski, P. J. Poole, R. L. Williams, D. Dalacu, *Sci. Rep.* **2022**, *12*, 6376.
[46] H. Y. Hui, R. B. Liu, *Phys. Rev. B* **2008**, *78*, 155315.
[47] V. S. Malinovsky, J. L. Krause, *Eur. Phys. J. D* **2001**, *14*, 147.

[48] S. Lüker, K. Gawarecki, D. E. Reiter, A. Grodecka-Grad, V. M. Axt, P. Machnikowski, T. Kuhn, *Phys. Rev. B* **2012**, *85*, 121302.
[49] T. Kaldewey, S. Lüker, A. V. Kuhlmann, S. R. Valentin, J.-M. Chauveau, A. Ludwig, A. D. Wieck, D. E. Reiter, T. Kuhn, R. J. Warburton, *Phys. Rev. B* **2017**, *95*, 241306.
[50] A. Ramachandran, G. R. Wilbur, S. O'Neal, D. G. Deppe, K. C. Hall, *Opt. Lett.* **2020**, *45*, 6498.
[51] M. Ghosh, R. Sharma, S. Bhattacharyya, *Chem. Phys. Lett.* **2007**, *449*, 165.
[52] Y. J. Wei, Y. M. He, M. C. Chen, Y. N. Hu, Y. He, D. Wu, C. Schneider, M. Kamp, S. Höfling, C. Y. Lu, J. W. Pan, *Nano Lett.* **2014**, *14*, 6515.
[53] V. Remesh, R. G. Krämer, R. Schwarz, F. Kappe, Y. Karli, M. P. Siems, T. K. Bracht, S. F. Covre da Silva, A. Rastelli, D. E. Reiter, D. Richter, S. Nolte, G. Weihs, *APL Photonics* **2023**, *8*, 101301.
[54] A. Ramachandran, J. Fraser-Leach, S. O'Neal, D. G. Deppe, K. C. Hall, *Opt. Express* **2021**, *29*, 41766.
[55] A. Ramachandran, G. R. Wilbur, R. Mathew, A. Mason, S. O. Neal, D. G. Deppe, K. C. Hall, arXiv preprint arXiv:2311.16982 (**2023**).
[56] L. Hanschke, K. A. Fischer, S. Appel, D. Lukin, J. Wierzbowski, S. Sun, R. Trivedi, J. Vuckovic, J. J. Finley, K. Muller, *npj Quantum Inf.* **2018**, *4*, 43.
[57] M. Cygorek, M. Cosacchi, A. Vagov, V. M. Axt, B. W. Lovett, J. Keeling, E. M. Gauger, *Nat. Phys.* **2022**, *18*, 662.
[58] A. Strathearn, P. Kirton, D. Kilda, J. Keeling, B. W. Lovett, *Nat. Commun* **2018**, *9*, 3322.
[59] M. R. Jørgensen, F. A. Pollock, *Phys. Rev. Lett.* **2019**, *123*, 240602.
[60] F. A. Pollock, C. Rodríguez-Rosario, T. Frauenheim, M. Paternostro, K. Modi, *Phys. Rev. A* **2018**, *97*, 012127.
[61] M. Cosacchi, M. Cygorek, F. Ungar, A. M. Barth, A. Vagov, V. M. Axt, *Phys. Rev. B* **2018**, *98*, 125302.
[62] R. Mathew, C. E. Pryor, M. E. Flatté, K. C. Hall, *Phys. Rev. B* **2011**, *84*, 205322.
[63] M. Glässl, A. M. Barth, K. Gawarecki, P. Machnikowski, M. D. Croitoru, S. Lüker, D. E. Reiter, T. Kuhn, V. M. Axt, *Phys. Rev. B* **2013**, *87*, 085303.
[64] A. Debnath, C. Meier, B. Chatel, T. Amand, *Phys. Rev. B* **2013**, *88*, 201305.
[65] E. Schmidgall, P. Eastham, R. Phillips, *Phys. Rev. B* **2010**, *81*, 195306.
[66] K. Gawarecki, S. Lüker, D. E. Reiter, T. Kuhn, M. Glässl, V. M. Axt, A. Grodecka-Grad, P. Machnikowski, *Phys. Rev. B* **2012**, *86*, 235301.
[67] J. S. Melinger, A. Hariharan, S. R. Gandhi, W. S. Warren, *J. Chem. Phys.* **1991**, *95*, 2210.
[68] J. S. Melinger, S. R. Gandhi, A. Hariharan, J. X. Tull, W. S. Warren, *Phys. Rev. Lett.* **1992**, *68*, 2000.
[69] J. S. Melinger, S. R. Gandhi, A. Hariharan, D. Goswami, W. S. Warren, *J. Chem. Phys.* **1994**, *101*, 6439.
[70] B. Broers, H. B. van Linden van den Heuvell, L. D. Noordam, *Phys. Rev. Lett.* **1992**, *69*, 2062.
[71] T. Kaldewey, A. V. Kuhlmann, S. R. Valentin, A. Ludwig, A. D. Wieck, R. J. Warburton, *Nat. Photonics* **2018**, *12*, 68.
[72] A. Debnath, C. Meier, B. Chatel, T. Amand, *Phys. Rev. B* **2012**, *86*, 161304.
[73] G. R. Wilbur, A. Binai-Motlagh, A. Clarke, A. Ramachandran, N. Milson, J. P. Healey, S. O'Neal, D. G. Deppe, K. C. Hall, *APL Photonics* **2022**, *7*, 111302.
[74] N. Renaud, F. C. Grozema, *Phys. Rev. B* **2014**, *90*, 165307.
[75] C. Creatore, R. T. Brierley, R. T. Phillips, P. B. Littlewood, P. R. Eastham, *Phys. Rev. B* **2012**, *86*, 155442.
[76] S. Zhdanovich, E. A. Shapiro, M. Shapiro, J. W. Hepburn, V. Milner, *Phys. Rev. Lett.* **2008**, *100*, 103004.
[77] W. Sellmeier, *Ann. Phys.* **1871**, *219*, 272.
[78] M. Born, E. Wolf, *Principles of optics*, Cambridge University Press, Cambridge **1999**.
[79] M. Miranda, T. Fordell, C. Arnold, A. L'Huillier, H. Crespo, *Opt. Express* **2012**, *20*, 688.
[80] B. Alonso, Í. J. Sola, H. Crespo, *Sci. Rep.* **2018**, *8*, 3264.
[81] G. Steinmeyer, *Opt. Express* **2003**, *11*, 2385.
[82] R. Szipöcs, K. Ferencz, C. Spielmann, F. Krausz, *Opt. Lett.* **1994**, *19*, 201.
[83] E. Treacy, *IEEE J. Quantum Electron.* **1969**, *5*, 454.
[84] S. Backus, C. G. Durfee, M. M. Murnane, H. C. Kapteyn, *Rev. Sci. Instrum.* **1998**, *69*, 1207.
[85] O. Martinez, *IEEE J. Quantum Electron.* **1987**, *23*, 59.
[86] O. E. Martinez, *J. Opt. Soc. Am. B* **1986**, *3*, 929.
[87] O. E. Martinez, *IEEE J. Quantum Electron.* **1988**, *24*, 2530.
[88] A. Kostenbauder, *IEEE J. Quantum Electron.* **1990**, *26*, 1148.
[89] M. Lai, S. T. Lai, C. Swinger, *Appl. Opt.* **1994**, *33*, 6985.
[90] *Patent* **2014**.
[91] M. Lipka, M. Parniak, *arXiv preprint arXiv:2307.01141* **2023**.
[92] J. P. Heritage, A. M. Weiner, R. N. Thurston, *Opt. Lett.* **1985**, *10*, 609.
[93] R. Thurston, J. Heritage, A. Weiner, W. Tomlinson, *IEEE J. Quantum Electron.* **1986**, *22*, 682.
[94] Y. Tang, C. Hooker, O. Chekhlov, S. Hawkes, J. Collier, P. P. Rajeev, *Opt. Express* **2014**, *22*, 29363.
[95] K. Osvay, I. N. Ross, *Opt. Commun.* **1994**, *105*, 271.
[96] K. Osvay, A. Kovacs, Z. Heiner, G. Kurdi, J. Klebniczki, M. Csatari, *IEEE J. Sel. Top. Quantum Electron.* **2004**, *10*, 213.
[97] B. Webb, M. Guardalben, C. Dorrer, S. Bucht, J. Bromage, *Appl. Opt.* **2019**, *58*, 234.
[98] Z. Zhong, W. Gong, H. Jiang, H. Gu, X. Chen, S. Liu, *Appl. Sci.* **2020**, *10*, 1584.
[99] K. Chesnut, C. Barty, *Opt. Express* **2023**, *31*, 5687.
[100] Y. Zhao, F. Wu, C. Wang, J. Hu, Z. Zhang, X. Liu, X. Wang, X. Yang, P. Bai, H. Chen, J. Qian, J. Gui, Y. Li, Y. Liu, X. Lu, Y. Xu, Y. Leng, R. Li, *Appl. Phys. B* **2023**, *129*, 53.
[101] P. Kostryukov, *J. Opt. Soc. Am. B* **2021**, *38*, 1942.
[102] Z. Zhang, T. Yagi, *J. Appl. Phys.* **1995**, *77*, 937.
[103] G. Pretzler, A. Kasper, K. Witte, *Appl. Phys. B* **2000**, *70*, 1.
[104] C. Fiorini, C. Sauteret, C. Rouyer, N. Blanchot, S. Seznec, A. Migus, *IEEE J. Quantum Electron.* **1994**, *30*, 1662.
[105] Z. Li, S. Tokita, S. Matsuo, K. Sueda, T. Kurita, T. Kawasima, N. Miyanaga, *Opt. Express* **2017**, *25*, 21201.
[106] F. Liu, X. Liu, Z. Wang, J. Ma, X. Liu, L. Zhang, J. Wang, S. Wang, X. Lin, Y. Li, L. Chen, Z. Wei, J. Zhang, *Appl. Phys. B* **2010**, *101*, 587.
[107] A. M. Weiner, *Rev. Sci. Instrum.* **2000**, *71*, 1929.
[108] Z. Zhang, Z. You, D. Chu, *Light Sci. Appl.* **2014**, *3*, e213.
[109] A. Gamouras, R. Mathew, S. Freisem, D. G. Deppe, K. C. Hall, *Nano Lett.* **2013**, *13*, 4666.
[110] A. Weigel, A. Sebesta, P. Kukura, *J. Phys. Chem. Lett.* **2015**, *6*, 4032.
[111] N. Accanto, P. M. De Roque, M. Galvan-Sosa, S. Christodoulou, I. Moreels, N. F. Van Hulst, *Light Sci. Appl.* **2017**, *6*, e16239.
[112] J. C. Vaughan, T. Hornung, T. Feurer, K. A. Nelson, *Opt. Lett.* **2005**, *30*, 323.
[113] E. Frumker, Y. Silberberg, *J. Opt. Soc. Am. B* **2007**, *24*, 2940.
[114] E. Frumker, Y. Silberberg, *J. Mod. Opt.* **2009**, *56*, 2049.
[115] H. Takahashi, Y. Kawada, H. Satozono, K. Takahashi, K. Watanabe, T. Inoue, H. Takahashi, *Opt. Express* **2019**, *27*, 25305.
[116] L. Serino, J. Gil-Lopez, M. Stefszky, R. Ricken, C. Eigner, B. Brecht, C. Silberhorn, *PRX Quantum* **2023**, *4*, 020306.
[117] A. Efimov, M. D. Moores, B. Mei, J. Krause, C. Siders, D. Reitze, *Appl. Phys. B* **2000**, *70*, S133.
[118] H. Takahashi, K. Watanabe, K. Shigematsu, T. Inoue, H. Satozono, *Opt. Continuum* **2023**, *2*, 1053.
[119] L. Xu, N. Nakagawa, R. Morita, H. Shigekawa, M. Yamashita, *IEEE J. Quantum Electron.* **2000**, *36*, 893.
[120] M. M. Wefers, K. A. Nelson, *J. Opt. Soc. Am. B* **1995**, *12*, 1343.
[121] M. M. Wefers, K. A. Nelson, *IEEE J. Quantum Electron.* **1996**, *32*, 161.

[122] T. Tanabe, H. Tanabe, Y. Teramura, F. Kannari, *J. Opt. Soc. Am. B* **2002**, *19*, 2795.
[123] T. Tanab, F. Kannari, F. Korte, J. Koch, B. Chichkov, *Appl. Opt.* **2005**, *44*, 1092.
[124] J. C. Vaughan, T. Feurer, K. W. Stone, K. A. Nelson, *Opt. Express* **2006**, *14*, 1314.
[125] B. J. Sussman, R. Lausten, A. Stolow, *Phys. Rev. A* **2008**, *77*, 043416.
[126] S. W. Jolly, O. Gobert, F. Quéré, *J. Opt.* **2020**, *22*, 103501.
[127] Y. Karli, F. Kappe, V. Remesh, T. K. Bracht, J. Munzberg, S. Covre da Silva, T. Seidelmann, V. M. Axt, A. Rastelli, D. E. Reiter, G. Weihs, *Nano Lett.* **2022**, *22*, 6567.
[128] I. Akimov, J. Andrews, F. Henneberger, *Phys. Rev. Lett.* **2006**, *96*, 067401.
[129] D. Brinks, R. Hildner, F. D. Stefani, N. F. van Hulst, *Opt. Express* **2011**, *19*, 26486.
[130] B. Xu, J. M. Gunn, J. M. D. Cruz, V. V. Lozovoy, M. Dantus, *JOSA B* **2006**, *23*, 750.
[131] N. Accanto, J. B. Nieder, L. Piatkowski, M. Castro-Lopez, F. Pastorelli, D. Brinks, N. F. van Hulst, *Light Sci. Appl.* **2014**, *3*, e143.
[132] S. Moser, M. Ritsch-Marte, G. Thalhammer, *Opt. Express* **2019**, *27*, 25046.
[133] Datasheet, Modulation of ultrashort laser pulses using slm-s liquid crystal spatial light modulators fromJenoptik, *Jenoptik Website*.
[134] Datasheet, Hamamatsu photonics, *LCOS-SLM X15213 series* **2022**.
[135] J. W. Wilson, P. Schlup, R. A. Bartels, *Opt. Express* **2007**, *15*, 8979.
[136] J. Pupeikis, N. Bigler, S. Hrisafov, C. R. Phillips, U. Keller, *Opt. Express* **2019**, *27*, 175.
[137] G.-H. Lee, S. Xiao, A. M. Weiner, *IEEE Photonics Technol.* **2006**, *18*, 1819.
[138] A. J. Metcalf, V. Supradeepa, D. E. Leaird, A. M. Weiner, *Opt. Express* **2013**, *21*, 28029.
[139] V. Supradeepa, E. Hamidi, D. E. Leaird, A. M. Weiner, *J. Opt. Soc. Am. B* **2010**, *27*, 1833.
[140] M. Martyanov, I. Mukhin, I. Kuzmin, S. Mironov, *Opt. Lett.* **2022**, *47*, 557.
[141] S. Mansha, P. Moitra, X. Xu, T. W. W. Mass, R. M. Veetil, X. Liang, S.-Q. Li, R. Paniagua-Domínguez, A. I. Kuznetsov, *Light Sci. Appl.* **2022**, *11*, 141.
[142] C. Peng, R. Hamerly, M. Soltani, D. R. Englund, *Opt. Express* **2019**, *27*, 30669.
[143] S. Divitt, W. Zhu, C. Zhang, H. J. Lezec, A. Agrawal, *Science* **2019**, *364*, 890.
[144] D. Cruz-Delgado, S. Yerolatsitis, N. K. Fontaine, D. N. Christodoulides, R. Amezcua-Correa, M. A. Bandres, *Nat. Photon.* **2022**, *16*, 686.
[145] K. Wang, M. Chekhova, Y. Kivshar, *Physics Today* **2022**, *75*, 38.
[146] J. Thomas, C. Voigtlaender, R. G. Becker, D. Richter, A. Tuennermann, S. Nolte, *Laser Photonics Rev.* **2012**, *6*, 709.
[147] T. Erdogan, *J. Lightwave Technol.* **1997**, *15*, 1277.
[148] F. Ouellette, *Opt. Lett.* **1987**, *12*, 847.
[149] K. O. Hill, F. Bilodeau, B. Malo, T. Kitagawa, S. Thériault, D. C. Johnson, J. Albert, K. Takiguchi, *Opt. Lett.* **1994**, *19*, 1314.
[150] G. Imeshev, I. Hartl, M. Fermann, *Opt. Express* **2004**, *12*, 6508.
[151] G. Imeshev, I. Hartl, M. Fermann, *Opt. Lett.* **2004**, *29*, 679.
[152] J. Gan, Y. Hao, Q. Ye, Z. Pan, H. Cai, R. Qu, Z. Fang, *Opt. Lett.* **2011**, *36*, 879.
[153] P. Saccomandi, A. Varalda, R. Gassino, D. Tosi, C. Massaroni, M. A. Caponero, R. Pop, S. Korganbayev, G. Perrone, M. Diana, A. Vallan, G. Costamagna, J. Marescaux, E. Schena, *J. Biomed. Opt.* **2017**, *22*, 097002.
[154] K. Markowski, K. Jędrzejewski, M. Marzęcki, T. Osuch, *Opt. Lett.* **2017**, *42*, 1464.
[155] P. Wei, H. Lang, T. Liu, D. Xia, *Sensors* **2017**, *17*, 2552.
[156] A. O. C. Davis, P. M. Saulnier, M. Karpiński, B. J. Smith, *Opt. Express* **2017**, *25*, 12804.
[157] F. Sośnicki, M. Mikołajczyk, A. Golestani, M. Karpiński, *Nat. Photonics* **2023**, *17*, 761.
[158] B. J. Eggleton, P. A. Krug, L. Poladian, K. Ahmed, H.-F. Liu, *Opt. Lett.* **1994**, *19*, 877.
[159] C. Wang, J. Yao, *IEEE Photonics Technol. Lett.* **2009**, *21*, 1375.
[160] M. Li, J. Yao, *IEEE Photonics Technol. Lett.* **2011**, *23*, 1439.
[161] T. O. Imogore, R. G. Krämer, T. A. Goebel, C. Matzdorf, D. Richter, S. Nolte, *Opt. Lett.* **2020**, *45*, 6526.
[162] D. B. Northeast, D. Dalacu, J. F. Weber, J. Phoenix, J. Lapointe, G. C. Aers, P. J. Poole, R. L. Williams, *Sci. Rep.* **2021**, *11*, 22878.
[163] D. Cadeddu, J. Teissier, F. R. Braakman, N. Gregersen, P. Stepanov, J.-M. Gérard, J. Claudon, R. J. Warburton, M. Poggio, M. Munsch, *Appl. Phys. Lett.* **2016**, *108*, 011112.
[164] K. Żołnacz, A. Musiał, N. Srocka, J. Große, M. J. Schlösinger, P.-I. Schneider, O. Kravets, M. Mikulicz, J. Olszewski, K. Poturaj, G. Wójcik, P. Mergo, K. Dybka, M. Dyrkacz, M. Dłubek, S. Rodt, S. Burger, L. Zschiedrich, G. Sęk, S. Reitzenstein, W. Urbańczyk, *Opt. Express* **2019**, *27*, 26772.
[165] T. Gao, L. Rickert, F. Urban, J. Große, N. Srocka, S. Rodt, A. Musial, K. Żołnacz, P. Mergo, K. Dybka, W. Urbańczyk, G. Sek, S. Burger, S. Reitzenstein, T. Heindel, *Appl. Phys. Rev.* **2022**, *9*, 011412.
[166] R. S. Daveau, K. C. Balram, T. Pregnolato, J. Liu, E. H. Lee, J. D. Song, V. Verma, R. Mirin, S. W. Nam, L. Midolo, S. Stobbe, K. Srinivasan, P. Lodahl, *Optica* **2017**, *4*, 178.
[167] M. Gagné, S. Loranger, J. Lapointe, R. Kashyap, *Opt. Express* **2014**, *22*, 387.
[168] D. N. Schimpf, E. Seise, J. Limpert, A. Tünnermann, *Opt. Express* **2008**, *16*, 10664.
[169] K. O. Hill, G. Meltz, *J. Light. Technol.* **1997**, *15*, 1263.
[170] B. J. Eggleton, J. A. Rogers, P. S. Westbrook, T. A. Strasser, *IEEE Photon. Technol. Lett.* **1999**, *11*, 854.
[171] G. P. Agrawal, in *Nonlinear Fiber Optics*, Academic Press, San Diego **2012**.
[172] B. R. Washburn, J. A. Buck, S. E. Ralph, *Opt. Lett.* **2000**, *25*, 445.
[173] M. L. Åslund, N. Jovanovic, N. Groothoff, J. Canning, G. D. Marshall, S. D. Jackson, A. Fuerbach, M. J. Withford, *Opt. Express* **2008**, *16*, 14248.
[174] L. B. Glebov, V. Smirnov, E. Rotari, I. Cohanoschi, L. Glebova, O. V. Smolski, J. Lumeau, C. Lantigua, A. Glebov, *Opt. Eng.* **2014**, *53*, 051514.
[175] M. Nejbauer, T. M. Kardaś, Y. Stepanenko, C. Radzewicz, *Opt. Lett.* **2016**, *41*, 2394.
[176] E. A. Perevezentsev, M. P. Siems, D. Richter, I. B. Mukhin, R. G. Krämer, A. I. Gorokhov, M. R. Volkov, S. Nolte, *Opt. Express* **2023**, *31*, 14286.
[177] D. Štěpánková, J. Mužík, O. Novák, L. Roškot, V. Smirnov, L. Glebov, M. Jelínek, M. Smrž, A. Lucianetti, T. Mocek, *Appl. Opt.* **2020**, *59*, 7938.
[178] K.-H. Liao, M.-Y. Cheng, E. Flecher, V. I. Smirnov, L. B. Glebov, A. Galvanauskas, *Opt. Express* **2007**, *15*, 4876.
[179] O. Mhibik, M. Yessenov, L. Mach, L. Glebov, A. F. Abouraddy, I. Divliansky, *Opt. Lett.* **2023**, *48*, 1180.
[180] S. Tang, T. B. Krasieva, Z. Chen, G. Tempea, B. J. Tromberg, *J. Biomed. Opt.* **2006**, *11*, 020501.
[181] V. Remesh, M. Stührenberg, L. Saemisch, N. Accanto, N. F. van Hulst, *Appl. Phys. Lett.* **2018**, *113*, 21.
[182] J.-C. Diels, W. Rudolph, *Ultrashort laser pulse phenomena*, Academic Press, San Diego **2006**.
[183] J. K. Ranka, A. L. Gaeta, A. Baltuska, M. S. Pshenichnikov, D. A. Wiersma, *Opt. Lett.* **1997**, *22*, 1344.
[184] E. Chong, T. Watson, F. Festy, *Appl. Phys.* **2014**, *105*, 062111.

[185] N. F. Kleimeier, T. Haarlammert, H. Witte, U. Schühle, J.-F. Hochedez, A. BenMoussa, H. Zacharias, *Opt. Express* **2010**, *18*, 6945.
[186] K. Naganuma, K. Mogi, H. Yamada, *IEEE J. Quantum Electron.* **1989**, *25*, 1225.
[187] R. Trebino, K. W. DeLong, D. N. Fittinghoff, J. N. Sweetser, M. A. Krumbügel, B. A. Richman, D. J. Kane, *Rev. Sci. Instrum.* **1997**, *68*, 3277.
[188] S. Linden, H. Giessen, J. Kuhl, *Phys. Status Solidi B* **1998**, *206*, 119.
[189] P. O'Shea, M. Kimmel, X. Gu, R. Trebino, *Opt. Lett.* **2001**, *26*, 932.
[190] G. Stibenz, G. Steinmeyer, *Opt. Express* **2005**, *13*, 2617.
[191] C. Iaconis, I. A. Walmsley, *Opt. Lett.* **1998**, *23*, 792.
[192] P. Bowlan, P. Gabolde, A. Shreenath, K. McGresham, R. Trebino, S. Akturk, *Opt. Express* **2006**, *14*, 11892.
[193] L. Lepetit, G. Chériaux, M. Joffre, *J. Opt. Soc. Am. B* **1995**, *12*, 2467.
[194] J.-P. Geindre, P. Audebert, S. Rebibo, J.-C. Gauthier, *Opt. Lett.* **2001**, *26*, 1612.
[195] C. Sainz, P. Jourdian, R. Escalona, J. Calatroni, *Opt. Commun.* **1994**, *110*, 381.
[196] A. Kovács, K. Osvay, G. Kurdi, M. Görbe, J. Klebniczki, Z. Bor, *Appl. Phys. B* **2005**, *80*, 165.
[197] W. Fan, B. Zhu, Y. Wu, F. Qian, M. Shui, S. Du, B. Zhang, Y. Wu, J. Xin, Z. Zhao, L. Cao, Y. Wang, Y. Gu, *Opt. Express* **2013**, *21*, 13062.
[198] F. B. Basset, M. B. Rota, C. Schimpf, D. Tedeschi, K. D. Zeuner, S. C. Da Silva, M. Reindl, V. Zwiller, K. D. Jöns, A. Rastelli, R. Trotta, *Phys. Rev. Lett.* **2019**, *123*, 160501.
[199] C. H. Bennett, G. Brassard, *Theor. Comput. Sci.* **2014**, *560*, 7.
[200] S. Ates, I. Agha, A. Gulinatti, I. Rech, M. T. Rakher, A. Badolato, K. Srinivasan, *Phys. Rev. Lett.* **2012**, *109*, 147405.
[201] A. Singh, Q. Li, S. Liu, Y. Yu, X. Lu, C. Schneider, S. Höfling, J. Lawall, V. Verma, R. Mirin, S. W. Nam, J. Liu, K. Srinivasan, *Optica* **2019**, *6*, 563.
[202] J. H. Weber, B. Kambs, J. Kettler, S. Kern, J. Maisch, H. Vural, M. Jetter, S. L. Portalupi, C. Becher, P. Michler, *Nat. Nanotechnol.* **2019**, *14*, 23.
[203] X. You, M.-Y. Zheng, S. Chen, R.-Z. Liu, J. Qin, M.-C. Xu, Z.-X. Ge, T.-H. Chung, Y.-K. Qiao, Y.-F. Jiang, H.-S. Zhong, M.-C. Chen, H. Wang, Y.-M. He, X.-P. Xie, H. Li, L.-X. You, C. Schneider, J. Yin, T.-Y. Chen, M. Benyoucef, Y.-H. Huo, S. Höfling, Q. Zhang, C.-Y. Lu, J.-W. Pan, *Adv. Photon.* **2022**, *4*, 066003.
[204] V. Giesz, S. Portalupi, T. Grange, C. Antón, L. De Santis, J. Demory, N. Somaschi, I. Sagnes, A. Lemaître, L. Lanco, A. Auffeves, P. Senellart, *Phys. Rev. B* **2015**, *92*, 161302.
[205] T. Santiago-Cruz, A. Fedotova, V. Sultanov, M. A. Weissflog, D. Arslan, M. Younesi, T. Pertsch, I. Staude, F. Setzpfandt, M. Chekhova, *Nano Lett.* **2021**, *21*, 4423.
[206] T. Santiago-Cruz, S. D. Gennaro, O. Mitrofanov, S. Addamane, J. Reno, I. Brener, M. V. Chekhova, *Science* **2022**, *377*, 991.
[207] Ł. Dusanowski, D. Kock, C. Schneider, S. Hofling, *ACS Photonics* **2023**, *10*, 2941.
[208] P. Laferriere, E. Yeung, L. Giner, S. Haffouz, J. Lapointe, G. C. Aers, P. J. Poole, R. L. Williams, D. Dalacu, *Nano Lett.* **2020**, *20*, 3688.
[209] H. Wang, Y. He, Y.-H. Li, Z.-E. Su, B. Li, H.-L. Huang, X. Ding, M.-C. Chen, C. Liu, J. Qin, J.-P. Li, Y.-M. He, C. Schneider, M. Kamp, C.-Z. Peng, S. Höfling, C.-Y. Lu, J.-W. Pan, *Nat. Photon.* **2017**, *11*, 361.
[210] J. C. Loredo, M. A. Broome, P. Hilaire, O. Gazzano, I. Sagnes, A. Lemaitre, M. P. Almeida, P. Senellart, A. G. White, *Phys. Rev. Lett.* **2017**, *118*, 130503.
[211] F. B. Basset, M. Valeri, E. Roccia, V. Muredda, D. Poderini, J. Neuwirth, N. Spagnolo, M. B. Rota, G. Carvacho, F. Sciarrino, R. Trotta, *Sci. Adv.* **2021**, *7*, eabe6379.
[212] M. Bozzio, M. Vyvlecka, M. Cosacchi, C. Nawrath, T. Seidelmann, J. C. Loredo, S. L. Portalupi, V. M. Axt, P. Michler, P. Walther, *npj Quantum Inf.* **2022**, *8*, 104.
[213] J. Azana, M. A. Muriel, *Opt. Lett.* **1999**, *24*, 1672.
[214] R. Mathew, H. Y. S. Yang, K. C. Hall, *Phys. Rev. B* **2015**, *92*, 155306.
[215] A. Javadi, N. Tomm, N. O. Antoniadis, A. J. Brash, R. Schott, S. R. Valentin, A. D. Wieck, A. Ludwig, R. J. Warburton, *New J. Phys.* **2023**, *25*, 093027.
[216] I. L. Medintz, H. T. Uyeda, E. R. Goldman, H. Mattoussi, *Nat. Mater.* **2005**, *4*, 435.
[217] F. P. García de Arquer, D. V. Talapin, V. I. Klimov, Y. Arakawa, M. Bayer, E. H. Sargent, *Science* **2021**, *373*, eaaz8541.
[218] E. Betzig, G. H. Patterson, R. Sougrat, O. W. Lindwasser, S. Olenych, J. S. Bonifacino, M. W. Davidson, J. Lippincott-Schwartz, H. F. Hess, *Science* **2006**, *313*, 1642.
[219] M. J. Rust, M. Bates, X. Zhuang, *Nat. Methods* **2006**, *3*, 793.
[220] X. Qu, D. Wu, L. Mets, N. F. Scherer, *Proc. Natl. Acad. Sci.* **2004**, *101*, 11298.
[221] W. E. Moerner, L. Kador, *Phys. Rev. Lett.* **1989**, *62*, 2535.
[222] S. W. Hell, J. Wichmann, *Opt. Lett.* **1994**, *19*, 780.
[223] T. A. Klar, S. W. Hell, *Opt. Lett.* **1999**, *24*, 954.
[224] S. W. Hell, *Science* **2007**, *316*, 1153.
[225] I. Gerhardt, G. Wrigge, J. Hwang, G. Zumofen, V. Sandoghdar, *Phys. Rev. A* **2010**, *82*, 063823.
[226] C. Maurer, A. Jesacher, S. Bernet, M. Ritsch-Marte, *Laser Photonics Rev.* **2011**, *5*, 81.
[227] G. Bautista, M. Kauranen, *ACS Photonics* **2016**, *3*, 1351.
[228] C. Matthiesen, A. N. Vamivakas, M. Atatüre, *Phys. Rev. Lett.* **2012**, *108*, 093602.
[229] R. Fiolka, M. Beck, A. Stemmer, *Opt. Lett.* **2008**, *33*, 1629.
[230] A. L. Efros, L. E. Brus, *ACS Nano* **2021**, *15*, 6192.
[231] S. Lüker, T. Kuhn, D. Reiter, *Phys. Rev. B* **2015**, *92*, 201305.
[232] I. Schwartz, D. Cogan, E. R. Schmidgall, Y. Don, L. Gantz, O. Kenneth, N. H. Lindner, D. Gershoni, *Science* **2016**, *354*, 434.
[233] S. Germanis, P. Atkinson, R. Hostein, S. Majrab, F. Margaillan, M. Bernard, V. Voliotis, B. Eble, *Phys. Rev. B* **2021**, *104*, 115306.
[234] E. Poem, Y. Kodriano, C. Tradonsky, N. Lindner, B. Gerardot, P. Petroff, D. Gershoni, *Nat. Phys.* **2010**, *6*, 993.
[235] M. Holtkemper, G. F. Quinteiro, D. E. Reiter, T. Kuhn, *Phys. Rev. Res.* **2021**, *3*, 013024.
[236] J. McFarlane, P. A. Dalgarno, B. D. Gerardot, R. H. Hadfield, R. J. Warburton, K. Karrai, A. Badolato, P. M. Petroff, *Appl. Phys. Lett.* **2009**, *94*, 093113.
[237] C. Simon, J.-P. Poizat, *Phys. Rev. Lett.* **2005**, *94*, 030502.
[238] M. Cosacchi, T. Seidelmann, A. Mielnik-Pyszczorski, M. Neumann, T. K. Bracht, M. Cygorek, A. Vagov, D. E. Reiter, V. M. Axt, *Adv. Quantum Technol.* **2022**, *5*, 2100131.
[239] M. Goryca, P. Plochocka, T. Kazimierczuk, P. Wojnar, G. Karczewski, J. Gaj, M. Potemski, P. Kossacki, *Phys. Rev. B* **2010**, *82*, 165323.
[240] Y. Huo, V. Křápek, O. Schmidt, A. Rastelli, *Phys. Rev. B* **2017**, *95*, 165304.